

5-25-94  
E8697

# Perfluoropolyalkylether Decomposition on Catalytic Aluminas

Wilfredo Morales  
*Lewis Research Center*  
*Cleveland, Ohio*

April 1994



National Aeronautics and  
Space Administration

# PERFLUOROPOLYALKYLETHER DECOMPOSITION ON CATALYTIC ALUMINAS

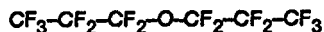
Wilfredo Morales, Sr.  
National Aeronautics and Space Administration  
Lewis Research Center  
Cleveland, Ohio 44135

## SUMMARY

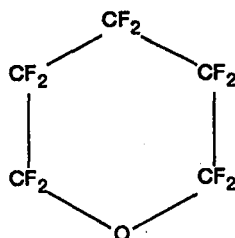
The decomposition of Fomblin Z25, a commercial perfluoropolyalkylether liquid lubricant, was studied using the Penn State Micro-oxidation Test, and a thermal gravimetric/differential scanning calorimetry unit. The micro-oxidation test was conducted using 440C stainless steel and pure iron metal catalyst specimens, whereas the thermal gravimetric/differential scanning calorimetry tests were conducted using catalytic alumina pellets. Analysis of the thermal data, high pressure liquid chromatography data, and x-ray photoelectron spectroscopy data support evidence that there are two different decomposition mechanisms for Fomblin Z25, and that reductive sites on the catalytic surfaces are responsible for the decomposition of Fomblin Z25.

## INTRODUCTION

Perfluoro-ethers are compounds consisting solely of carbon, oxygen, and fluorine atoms. The molecular structure of these compounds can be either linear or cyclic (fig. 1) and their molecular weights can vary from 254 to more than 15 000.



Linear Perfluoro-Ether



Cyclic Perfluoro-Ether

Figure 1.—Structures of typical linear and cyclic perfluoro-ether compounds.

In the 1960's (refs. 1 and 2) a class of perfluoro-ethers was synthesized that led to their extensive use by industry. This class is the perfluoropolyalkylethers (PFPE for short) and they can be considered to be low molecular weight liquid polymers. PFPE's are used as diffusion pump oils (refs. 3 and 4), dielectric fluids (ref. 5), and as lubricants (ref. 6).

Naturally, a substantial amount of work has been conducted investigating the physical and chemical properties of these liquids. Cantow et al. (ref. 7) investigated the molecular weight distributions of two different PFPE liquids using a light scattering technique. They were able to correlate the bulk viscosities of the PFPE liquids with the molecular weights.

Ouano and Appelt (ref. 8) also investigated the relationship between the viscosity and molecular weight of several PFPE's. In a different study, Cantow et al. (ref. 9) studied the viscosity variation of two different PFPE liquids. Recently, Pacansky et al. (ref. 10) employed computational quantum chemical methods to study the structures of model PFPE compounds.

A number of studies have emerged pertaining to the thermal stability of PFPE's. Jones et al. (ref. 11) investigated the thermal-oxidative degradation reactions of linear PFPE's. Helmick and Jones (ref. 12) used tensimetry to determine the thermal stability of PFPE's. Smart and Dixon (ref. 13) used a quantum chemical computer program to calculate C-F bond strengths of various perfluoro-ether model compounds. The surface chemistry of perfluoro-ethers has also been studied. Walczak et al. (ref. 14) looked at the decomposition of model perfluoro-ethers adsorbed on a Ru(001) surface. Napier and Stair (ref. 15) investigated the decomposition of three model perfluoro-ethers on iron surfaces. Herrera-Fierro et al. (ref. 16) used XPS and TDS to study the surface chemistry of a PFPE liquid on several metals.

Interest in the decomposition of perfluoro-ethers has not been limited to just thermal breakdown of these compounds. Pacansky et al. (ref. 17) used an electron beam to irradiate a perfluoro-ether and decompose it. D'Anna et al. (ref. 18) used an electron beam to study the stability of a PFPE liquid compared to two other hydrocarbon liquids. In another study, Pacansky and Waltman (ref. 19) irradiated several perfluoro-ethers with an electron beam and identified the gaseous products.

Irradiation of perfluoro-ethers by UV radiation has also been attempted. Ohtani et al. (ref. 20) studied the effects of UV radiation on thin films of a PFPE adsorbed on a gold surface. Saperstein and Lin (ref. 21) studied the surface adhesion of a PFPE following UV irradiation. In a similar study, Vurens et al. (ref. 22) studied the bonding between a PFPE and various substrates following UV irradiation.

An interesting study was conducted by Mori and Morales (ref. 23) whereby they irradiated several PFPE's with x-rays. They found, in several cases, that crosslinking of the PFPE's occurred. Mori and Morales (ref. 24) continued their work and were able to make x-ray photoelectron spectroscopy peak (XPS) assignments for several PFPE's.

A number of tribological studies, related to the use of PFPE's as liquid lubricants, has been conducted. Sianesi et al. (ref. 25) used a four-ball wear tester to study the lubricating properties of a PFPE. Snyder et al. (ref. 26) reported that linear PFPE's were excellent candidates for high-temperature wide-liquid range applications such as gas-turbine engine oils and hydraulic fluids. Jones and Snyder (ref. 27) used a ball-on-disk sliding friction apparatus to study the boundary lubricating characteristics of a PFPE to 573 K (300 °C). Cosmacini and Veronesi (ref. 28) investigated the tribological behavior of several PFPE's, using several different wear machines, and compared their performance to a hydrocarbon hydraulic oil. Morales and Buckley (ref. 29) studied the sliding friction and wear of several ceramics lubricated with a PFPE under concentrated contact conditions. D'Agostino et al. (ref. 30) investigated the tribological behavior of sintered iron bearings lubricated with a PFPE.

Other tribological studies using PFPE's center strongly on the use of PFPE's as lubricants for magnetic storage disk media (ref. 31). A thin layer ( $<75 \text{ \AA}$ ) of PFPE is coated onto the disk to provide lubrication between the disk and the head. PFPE's have also been studied as boundary lubricants for plastics (ref. 32).

NASA's interest in PFPE liquids stems from their use as space lubricants, as well as aerospace high temperature liquid lubricants. Several of the PFPE liquids have vapor pressures less than  $10^{-10}$  torr at room temperature; this property alone makes consideration of these liquids as space lubricants inevitable. Two particular types of PFPE's have been used on orbiting earth satellites (ref. 33) to lubricate the ball bearings of

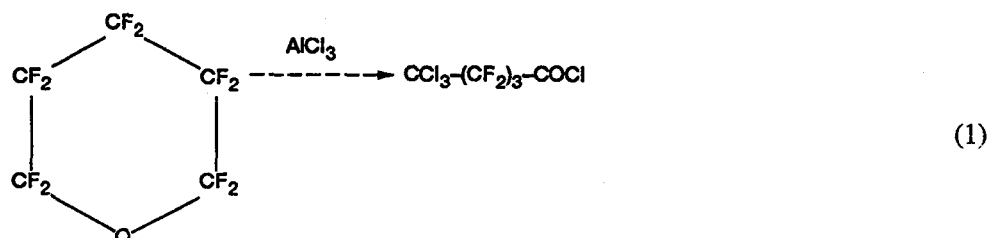
scanning equipment. One NASA report (ref. 34) detailed the anomalous behavior of a satellite scanner instrument and the authors concluded that the anomaly was apparently caused by a "lubrication problem." Since that report, several studies have been conducted on the tribological behavior of PFPE's under ultra-high vacuum conditions. In a series of experiments, Mori and Morales (refs. 35 and 36) investigated the decomposition and reaction of PFPE's with 440C stainless steel under pure sliding conditions in ultra-high vacuum. Masuko et al. (ref. 37) used a four-ball apparatus to investigate the lubricating properties of several PFPE's under high vacuum conditions.

NASA's interest in the use of PFPE's need not be limited solely to tribological applications. PFPE's have potential applications as heat transfer liquids (due to the thermal stability over a wide temperature range), mass transfer liquids (due to the large solubility of oxygen and carbon dioxide in PFPE's (ref. 38)), and as vibration damping liquids (PFPE's are much more compressible than conventional hydraulic liquids (ref. 39)). Most of these applications will require contact between the PFPE liquid and a solid surface, metal or ceramic. Thus, the successful use of PFPE's will depend, in part, on their stability when in contact with engineering surfaces.

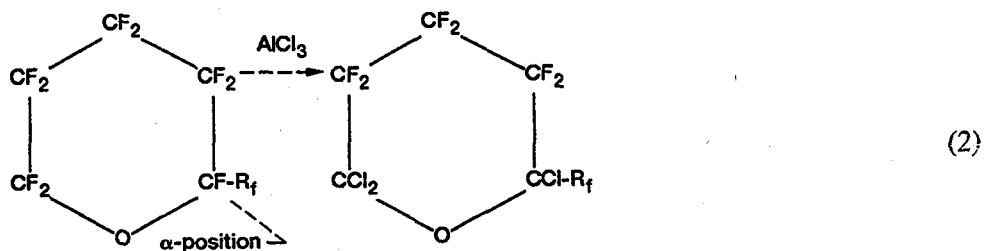
Of the commercially available PFPE's, one has drawn substantial attention. This PFPE is designated Fomblin Z25 and it shall be referred to as "PFPE F" throughout this dissertation. PFPE F has the lowest pour point, 207 K (-66 °C), among the commercial PFPE's and it also has the lowest vapor pressure ( $2.9 \cdot 10^{-12}$  torr at 293 K). In addition, PFPE F has the best viscometric properties based on viscosity-temperature slope measurements. Because of these properties, PFPE F is the lubricant of choice for many space applications. It has been found, however, that PFPE F tends to decompose more readily than the other PFPE's when in contact with certain engineering surfaces under certain conditions. In order to extend the operating life of PFPE F, the decomposition mechanism should be understood and a means of preventing decomposition (or at least reducing the rate of decomposition) must be addressed.

## BACKGROUND ON THE CHEMICAL DECOMPOSITION OF PERFLUORO-ETHERS

In 1955 Van Dyke Tiers published several articles (refs. 40 to 42) describing the chemical reactivity of two types of perfluoro-ethers, cyclic and linear, with  $\text{AlCl}_3$ . In one case he found that the cyclic ether,  $\text{C}_5\text{F}_{10}\text{O}$ , reacted with  $\text{AlCl}_3$  according to the following scheme:

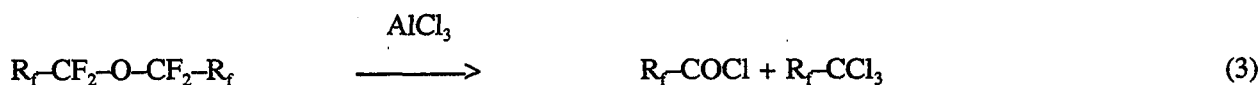


He also found, however, that if the cyclic perfluoro-ether contained a single perfluoroalkyl group ( $\text{R}_f$ ) in the  $\alpha$ -position, then the following reaction occurred:

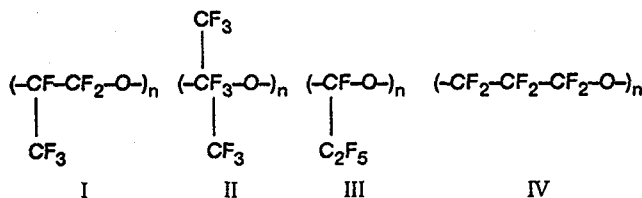


Reaction 1 is a substitution-cleavage reaction whereas reaction 2 is just a substitution reaction.

Van Dyke Tiers also demonstrated that a linear perfluoro-ether reacted with  $\text{AlCl}_3$  according to the following scheme:

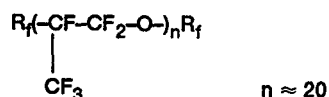


Sianesi and Fontanelli (ref. 43) also reacted perfluoro-ethers with  $\text{AlCl}_3$ . Instead of the simple perfluoro-ethers that Van Dyke Tiers used, Sianesi and Fontanelli were interested in the reaction of oligomers containing the repeating unit  $\text{-(C}_3\text{F}_6\text{O)-}$ . This repeating unit theoretically can have four different structures:



Sianesi and Fontanelli wanted to determine which structure the perfluoro-ether oligomers probably possessed. They reacted one oligomer having a number average molecular weight (MW) of 800 and a second oligomer having a MW of 1700. They collected and analyzed the reaction products, and based on the results reported by Van Dyke Tiers, concluded that the repeating unit of the polyether oligomers had structure I.

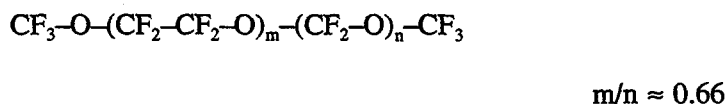
Carré and Markowitz (ref. 44) investigated the decomposition reaction of a perfluoropolyalkylether (PFPE K), which can be regarded as a low molecular weight liquid polyether polymer:



Their interest stemmed from the tribological use of PFPE K as a liquid lubricant. They reacted the PFPE K with  $FeF_3$  in an autoclave system under various conditions, and analyzed the reaction products. They concluded that  $FeF_3$  acts as a Lewis acid catalyst resulting in the decomposition of PFPE K. This conclusion was then used to support their proposed mechanism of PFPE K breakdown under lubricating conditions:

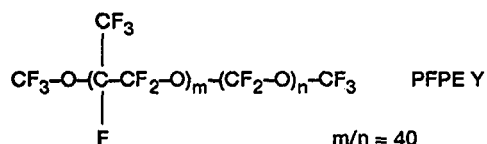
- (1) PFPE K interacts with steel surfaces to form  $FeF_3$ .
- (2)  $FeF_3$  then catalyzes the decomposition of PFPE K.

Zehe and Faut (ref. 45) conducted a decomposition experiment using PFPE F and  $\alpha-Fe_2O_3$ . The structure of PFPE F is shown below:



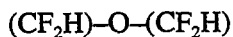
They reported that the decomposition of PFPE F proceeds in two stages. In the first stage, a slow catalytic reaction occurs between PFPE F and the  $\alpha-Fe_2O_3$  leading to the formation of  $FeF_3$ . In the second stage, the  $FeF_3$  then serves as a Lewis acid leading to the rapid catalytic decomposition of the PFPE F.

In a similar study, Kasai et al. (ref. 46) decomposed several PFPE's with  $\alpha-Al_2O_3$ . In addition to PFPE K and PFPE F, they also studied PFPE D and PFPE Y:



They found that PFPE F decomposed in the presence of  $\alpha\text{-Al}_2\text{O}_3$  at 473 K (200 °C), whereas PFPE D, K, and Y did not decompose. They concluded (as Jones and Paciorek concluded, ref. 11) that decomposition of PFPE F occurred due to the presence of acetal groups (-O-CF<sub>2</sub>-O-) in the molecule. They also concluded that the decomposition process proceeded in two stages, identical to that reported by Zehe and Faut (ref. 45): the slow formation of AlF<sub>3</sub> followed by the rapid Lewis acid catalytic decomposition of PFPE F.

Basu, Ballinger, and Yates (ref. 47) conducted an experiment where they adsorbed a model partially fluorinated ether compound



onto high surface area alumina ( $\gamma\text{-Al}_2\text{O}_3$ ). They conducted this experiment under ultra high vacuum conditions (pressure  $<1 \times 10^{-8}$  torr) at various temperatures. They reported that at 150 K (-123 °C) the fluoro-ether adsorbed on isolated surface hydroxyl groups without decomposing. They increased the temperature and found that the fluoro-ether started to desorb from the  $\gamma$ -alumina surface. At 250 K (-23 °C) most of the molecules desorbed from the surface. Above 250 K, a fraction of the remaining fluoro-ether molecules decomposed yielding a surface formate (HCOO). This experiment was repeated after using pyridine to block the Al<sup>3+</sup> Lewis acid sites. It was found that the fluoro-ether still decomposed to the surface formate. Basu et al. concluded that the Lewis acid sites and the hydroxyl groups were not responsible for the fluoro-ether decomposition. They postulated that an "oxygen center" was a possible site for the formate formation.

#### THE PENN STATE MICRO-OXIDATION TEST STUDY

The Penn State micro-oxidation test apparatus was used to study the decomposition of PFPE F (fig. 2). The main feature of this apparatus is the formation of a thin liquid film on a metal surface. The apparatus was designed with this feature in mind in order to minimize any effects of gaseous oxygen diffusion throughout the

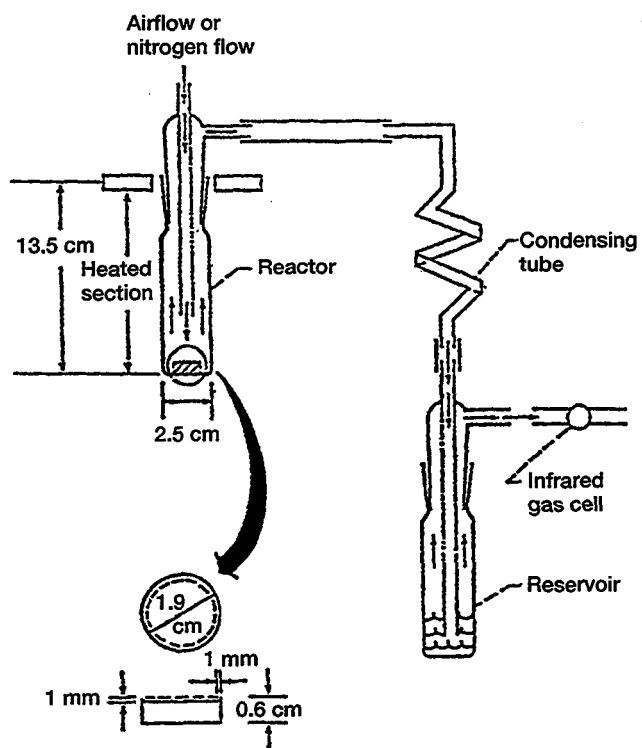


Figure 2.—Penn State micro-oxidation test apparatus.

liquid film (when a test was conducted in an air or oxygen atmosphere) in order to study reaction-controlled experiments. This apparatus was used to study the decomposition of ester based liquid lubricants (refs. 48 and 49) under various conditions, and the catalytic decomposition of thio-ether liquid lubricants (ref. 50). In addition to fast reaction test times (tests normally lasted 30 min or less), micro-oxidation test results were repeatable to within  $\pm 5$  percent of each other. Further details concerning the origin and concepts behind this particular test apparatus can be found in D.I.K.A. Ugwuzor, The Effect of Metals on High Temperature Degradation of Ester-Type Lubricants, Masters Thesis, Pennsylvania State University, 1982.

#### Micro-Oxidation Test Procedure

Three ml of PFPE F were degassed at 473 K (200 °C) and <5 torr for 30 min. The liquid was then eluted through a silica-filled column for removal of possible traces of water. Table I lists some of the physical properties of PFPE F.

TABLE I.—PROPERTIES OF FOMBLIN  
Z25 (PFPE F)

Average molecular weight	10 200
Kinematic viscosity at 20 °C, cS	255
Viscosity index	355
Pour point, °C	-66
Density at 20 °C, g/ml	1.851
Surface tension at 20 °, dyne/cm	25
Refractive index, $n_{20}^D$	1.294
Vapor pressure, torr	
At 20 °C	$2.9 \times 10^{-12}$
At 100 °C	$1.0 \times 10^{-8}$

The surfaces of the metal specimens were polished with diamond paste; this was followed by ultrasonic cleaning of the specimens in a beaker of 1,1,2-trichlorotrifluoroethane (TCF). The metal specimens were then rinsed with 200 proof ethanol and given a final polishing with alumina paste. The alumina paste was rinsed off with deionized water, and the specimens were dried in a nitrogen gas stream.

A metal specimen was then placed in the reactor section of the micro-oxidation apparatus, and 50  $\mu$ l of PFPE F was injected onto the metal surface. The entire apparatus was then purged with nitrogen gas (100 ml/min) for 30 min. This was followed by reducing the nitrogen gas flow rate to 20 ml/min and placing

the apparatus into a heating unit maintained at 618 K (345 °C)  $\pm$  1 K. This temperature was chosen based on previous experimentation that revealed PFPE F started to decompose at this temperature in a dry air atmosphere (20 ml/min flow rate) for a fixed test duration of 30 min. A 10-min heating period allowed the reactor portion of the micro-oxidation test apparatus to equilibrate at the test temperature. At the end of the 10-min equilibration period, the test atmosphere was either maintained with nitrogen or switched to air (both at 20 ml/min).

During the experiment, the reactor outlet was attached to a condensing tube (at room temperature), the outlet of which was attached to a reservoir containing 10 ml of TCF. This arrangement allowed the flowing test atmosphere to bubble into the TCF. At the end of a test (30-min test duration, not including the 10-min equilibration period), the micro-oxidation test apparatus was removed from the heating unit and allowed to cool to room temperature. Subsequently, all glassware was disconnected, and the contents of the reactor, the condensing tube, and the TCF reservoir were examined by using high pressure liquid chromatography (HPLC) in the size-exclusion mode—a separation mode whereby solute molecules are separated according to their molecular size (see appendix I for HPLC description and calibration).

Five ml of the TCF solvent were injected into the reactor so that the entire metal specimen was immersed. After a few minutes, the solvent was drawn off with a syringe and filtered through a 0.45- $\mu$ m nylon filter; 30  $\mu$ l of this filtered solution was injected into the HPLC unit for analysis.

The condensing tube contents were extracted with 3 ml of TCF, and the resulting solution was passed through a silica extraction cartridge. This procedure will allow nonpolar substances to elute with the TCF, whereas polar substances will be retained by the silica. The eluted TCF solution was then stored for HPLC analysis. Five ml of 200-proof ethanol were then passed through the silica extraction cartridge. The first 2 ml of the eluting ethanol were discarded, and the remaining 3 ml were collected and stored for chemical analysis. Polar substances, adsorbed on the silica, dissolved in the ethanol (a polar liquid) and eluted out of the cartridge. This procedure was repeated for the TCF reservoir.

All micro-oxidation tests were repeated a minimum of three times.

## Micro-Oxidation Test Results

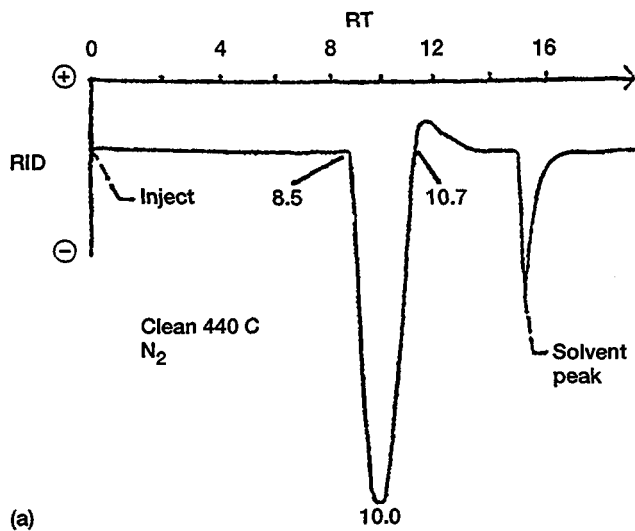
Figure 3(a) is the HPLC chromatogram of PFPE F remaining on the surface of the 440C stainless steel (SS) specimen at the end of the test, conducted under a flowing nitrogen atmosphere. Comparison with the pure, unreacted PFPE F (fig. 3(b)) shows no decomposition of the liquid.

In an air atmosphere, PFPE F completely decomposed; HPLC analysis revealed no liquid left on the 440C SS surface (fig. 4). The decomposition of PFPE F was accompanied by the formation of a liquid in the condensing tube and the bubbling of fumes into the TCF reservoir.

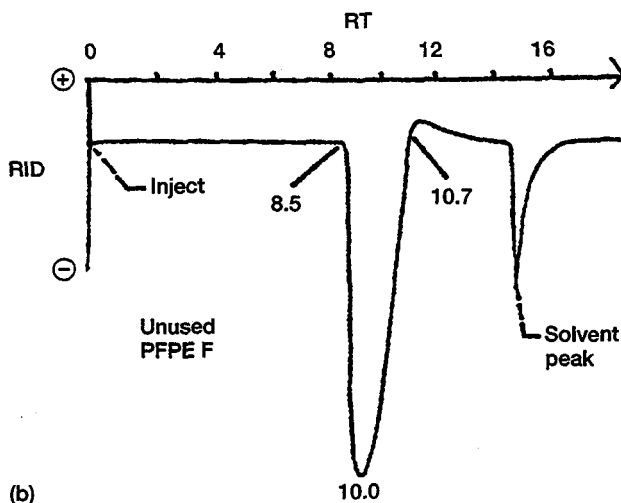
The liquid product in the condensing tube was extracted with TCF solvent and prepared for analysis as outlined in the Micro-Oxidation Test Procedure. HPLC analysis of the eluted TCF extract (fig. 5) revealed a product having a greater retention time (12.2 min) than PFPE F (10.0 min). Based on a calibration chart (see appendix I) relating the average molecular weights of known fluorinated substances to their retention times, the 12.2-min retention time corresponds an average molecular weight of about 1150.

HPLC analysis of the TCF reservoir revealed the presence of a product (fig. 6) at 18.4 min, several minutes past the solvent peak (14.4-min retention time); this indicated possible adsorption interaction with the column packing. By bubbling carbon dioxide gas into 5 ml of TCF solvent for a few minutes and immediately analyzing the solvent by HPLC (fig. 7), data was obtained which suggested that the eluted product at 18.4 min was carbon dioxide.

Figure 8 shows the Fourier transform infrared (FTIR) transmission spectra of undegraded PFPE F (neat between two NaCl windows) and the liquid product formed inside the condensing tube. The FTIR spectrum of the liquid product is similar to that of PFPE F; however, a strong sharp peak at  $1782\text{ cm}^{-1}$  and a broad peak between  $2650$  and  $3550\text{ cm}^{-1}$  are present in the FTIR spectrum of the liquid product. These bands correspond to carbonyl (C=O) and hydroxyl (OH) groups, respectively. To confirm the presence of these functional groups, the FTIR spectrum of a known diacid of PFPE F was taken. Figure 9 shows the molecular structure of the diacid and its FTIR spectrum.



(a)



(b)

Figure 3.—HPLC chromatograms of PFPE F remaining on surface of clean 440C specimen under  $N_2$  atmosphere, of unused PFPE F.

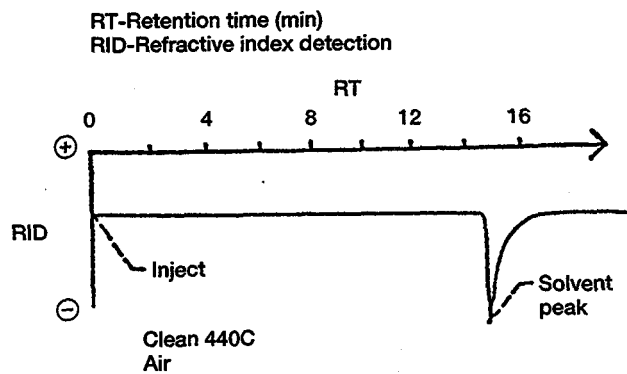


Figure 4.—HPLC chromatogram of PFPE F remaining on surface of clean 440C specimen under air atmosphere.

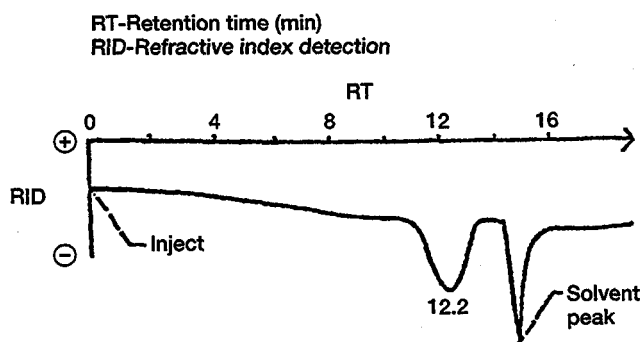


Figure 5.—HPLC chromatogram of liquid extracted from condensing tube. 440C specimen, air atmosphere.

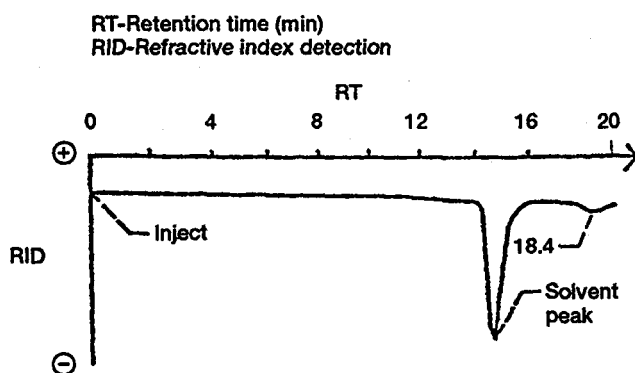


Figure 6.—HPLC chromatogram of reservoir contents.

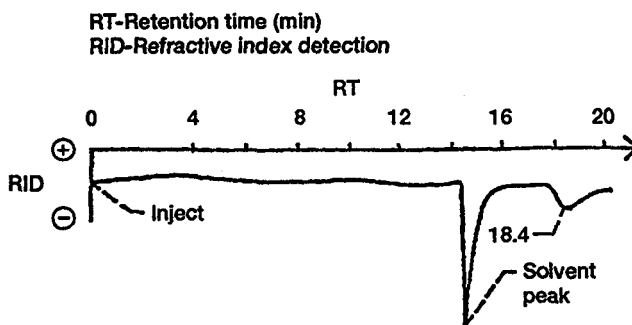


Figure 7.—HPLC chromatogram obtained by bubbling carbon dioxide gas into 5 ml 1,1,2 trichlorotrifluoroethane (TCF).

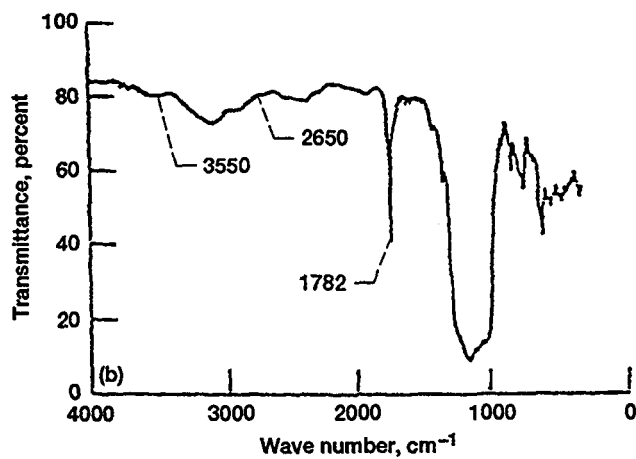
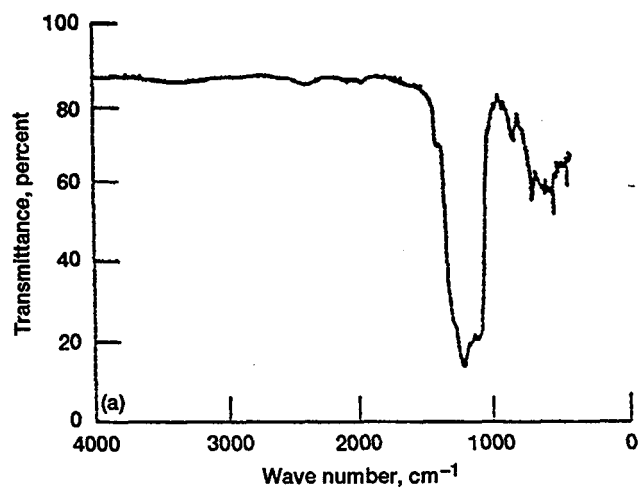


Figure 8.—FTIR spectra of PFPE F and liquid product extracted from condensing tube. (a) PFPE F. (b) Liquid product from condensing tube.



An FTIR spectrum (fig. 10) of the liquid product was also taken after eluting it through the silica extraction cartridge with TCF solvent. This spectrum shows two things: it is nearly identical to the FTIR spectrum of PFPE F, and the carbonyl and hydroxyl groups are absent. The evidence suggests that the liquid product formed in the condensing tube was not a single component. Therefore, the FTIR spectrum of the condensing tube product (fig. 8) appears to be a composite spectrum of at least two substances, one substance with a molecular structure very similar to that of PFPE F (but with a much lower molecular weight) and a second substance with a carboxylic acid functional group:

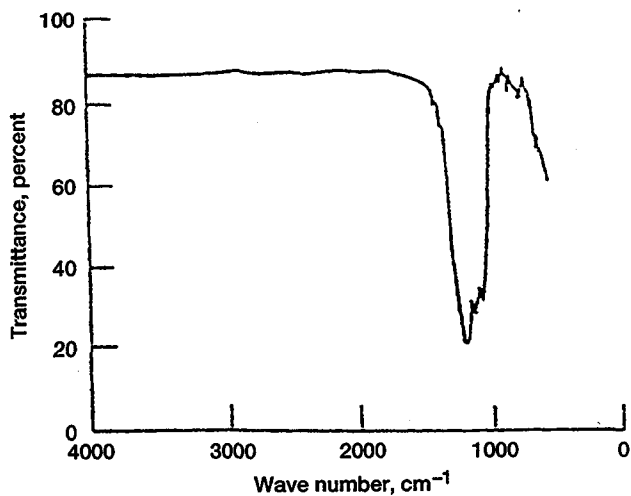
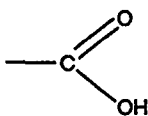


Figure 10.—FTIR spectrum of liquid product (from condensing tube) after elution through silica extraction cartridge.

During these tests, the outlet of the TCF reservoir was connected to an infrared (IR) gas cell, which allowed the collection of the fumes. Figure 11 is the FTIR spectrum of the fumes. In addition to the TCF solvent vapors, bands corresponding to carbon dioxide and carbonyl fluoride ( $\text{COF}_2$ ) are present.

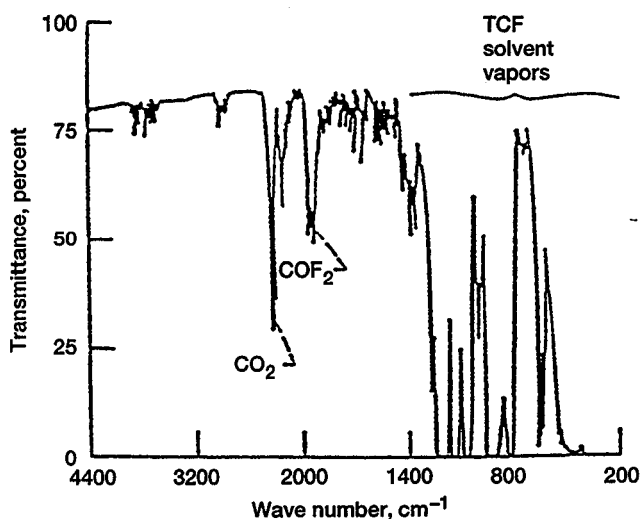


Figure 11.—FTIR spectrum of fumes collected in gas cell, showing 1,1,2 trichlorotrifluoroethane (TCF) solvent vapors, carbon dioxide ( $\text{CO}_2$ ), and carbonyl fluoride ( $\text{COF}_2$ ).

The 440C SS specimen, after being rinsed with TCF, revealed the presence of a fairly uniform brownish deposit on the surface.

The micro-oxidation test was repeated with an unused iron specimen, and it was found that PFPE F did not decompose under a flowing nitrogen atmosphere, but did decompose under a flowing air atmosphere. Unlike the test involving the 440C SS specimen, PFPE F decomposition was not complete (fig. 12). Not only was PFPE F decomposition incomplete, but repeatability of the results ( $\pm 5$  percent decomposition) could not be obtained. At the end of the first test, it was found that 72 percent of the liquid decomposed; three subsequent tests showed 87, 66, and 82 percent of the liquid decomposed.

Like the results obtained from the micro-oxidation test with the unused 440C SS specimen, a liquid collected in the condensing tube. HPLC and FTIR analysis revealed that the liquid had the same retention time and IR spectrum as the liquid from the 440C SS test. Analysis of the reservoir solution also showed a product

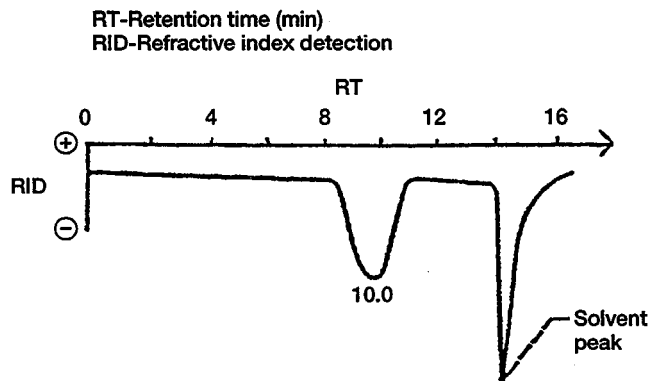


Figure 12.—HPLC chromatogram of PFPE F remaining on surface of clean iron specimen, air atmosphere.

(carbon dioxide) with the same retention time as the product from the 440C SS test. The surface of the iron specimen, after being rinsed with TCF, revealed a nonuniform brownish deposit.

#### Surface Analysis of Deposit

Surface analysis (electron spectroscopy for chemical analysis (ESCA)) of the used 440C SS specimen, with the brownish deposit, revealed iron and chromium compounds. The iron  $2p_{3/2}$  and chromium  $2p_{3/2}$  binding energies were consistent with the presence of iron oxide and chromium oxide ( $Cr_2O_3$ ). A fluorine  $1s$  line was also found in the spectrum. Its binding energy was consistent with a metal fluoride, but not a fluorocarbon.

The micro-oxidation test was repeated with PFPE F using a previously run 440C SS specimen covered with the brownish deposit (after rinsing the specimen with TCF solvent) in a flowing nitrogen atmosphere. It was found that 53 percent of the liquid decomposed.

Another series of micro-oxidation tests was conducted using clean 440C SS specimens. However, the specimen preparation was different for this series of tests. Instead of a final water rinse, TCF solvent was used as the final rinse. Table II lists and compares the decomposition percentages for both the TCF and water rinses.

TABLE II.—MICRO-OXIDATION TESTS FOR UNUSED IRON SPECIMENS

(a) With final TCF solvent rinse		(b) With final water rinse	
Test	Degradation, percent	Test	Degradation, percent
1	29	1	72
2	37	2	87
3	6	3	66
4	24	4	82

#### Micro-Oxidation Test Discussion

The micro-oxidation tests showed that certain conditions existed that led to the decomposition of PFPE F. It was observed that PFPE F did not decompose in the presence of the unused metal specimens in a nitrogen atmosphere at 618 K (345 °C) but the liquid did decompose in an air atmosphere with the generation of a brownish deposit on both the 440C SS and iron surfaces. Subsequent tests revealed that PFPE F then decomposed, in a nitrogen atmosphere, in the presence of the deposit.

It can be postulated that, in an air atmosphere, oxygen molecules diffuse through the thin PFPE F film and adsorb on the metal surface as an activated species. This activated oxygen species can then react with the iron forming iron oxide. The iron oxide then "catalyzes" the decomposition of PFPE F. The decomposition products can react with iron oxide (or iron) forming iron fluoride. The experimental evidence suggests that the presence of water is important in the decomposition process. Although valuable information was obtained about the decomposition of PFPE F using the micro-oxidation test, several drawbacks to the test were apparent. One was the lack of repeatability in the amount of PFPE F decomposed using the unused iron specimens. The other drawback was the high test temperature (618 K) needed to decompose PFPE F. Clearly, another test method was needed to study the decomposition of PFPE F.

#### THERMAL GRAVIMETRIC AND DIFFERENTIAL SCANNING CALORIMETRY STUDY

After consideration of several alternative test methods, it was decided that a thermal gravimetric analysis (TGA) unit combined with a differential scanning calorimetry (DSC) unit would meet the desired needs. In order to use these thermal units a means of introducing both PFPE F and the catalyst was needed. Impregnating a small cylindrical porous catalyst pellet with several microliters of PFPE F and then introducing the pellet into the thermal units was found to be a simple and efficient test procedure.

## TGA/DSC Test Procedure

Figure 13 shows the dimensions of the catalyst pellet used in the TGA unit. There were several reasons for using  $\text{Al}_2\text{O}_3$  ( $\alpha$  and  $\gamma$  forms) as the catalyst: (1) a review of the literature (ref. 46) suggested that PFPE F decomposition would occur at a lower temperature with alumina, (2)  $\gamma$   $\text{Al}_2\text{O}_3$  is known to form well defined Lewis acid sites after suitable pretreatment (ref. 51), and (3) a substantial amount of literature exists on the use of alumina as a catalyst. All alumina pellets were preheated, in the TGA unit, to 773 K (500 °C) under a flowing nitrogen atmosphere. After pretreatment, the pellets were stored under vacuum until needed.

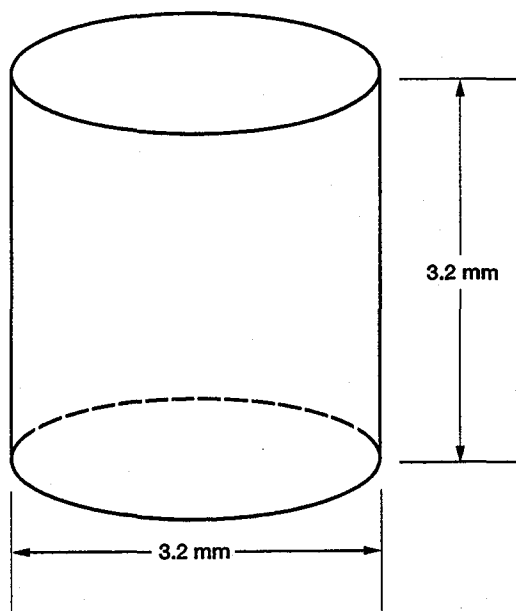


Figure 13.—Alumina catalyst pellet.

An alumina pellet was placed inside the TGA chamber and its mass was weighed. A microliter syringe was then used to inject a single drop of PFPE F (for all tests the drop measured  $5.0 \pm 0.5$  mg) onto the top flat surface of the pellet, and the pellet placed back into the TGA. The TGA was purged with nitrogen (70 ml/min) for 10 min prior to the start of a test. At the end of a TGA test, the alumina pellet was quickly removed from the TGA unit and immersed in a bottle containing 3 ml of TCF. After a 24-hr waiting period, 50  $\mu\text{l}$  of the TCF solvent was withdrawn from the bottle and injected into the HPLC system.

The TGA test was conducted initially in the following manner: (1) the temperature was ramped at 40 K/min from room temperature to 455 K (182 °C), (2) the temperature ramp was then immediately switched to 5 K/min to 473 K (200 °C), and (3) the TGA unit was then maintained isothermally at 473 K. This heating procedure was followed in order to bring the pellet to 473 K as quickly as possible without overshooting the target temperature. Difficulties were experienced using this procedure, so a second heating procedure was tried. After ramping the temperature from room temperature to 455 K at 40 K/min, the temperature ramp was again changed to 5 K/min. At 468 K (195 °C) the temperature ramp was changed to 1 K/min and this ramp was maintained till the completion of a test.

A series of tests was first conducted using  $\alpha$ -alumina pellets where the TGA temperature was ramped and maintained at 473 K. In the first test, 5 min elapsed before PFPE F started to decompose. The decomposition was allowed to go to completion. Based on the recorded weight measurement, nearly all the PFPE F decomposed.

Subsequent tests were conducted in order to assess the repeatability of this method. In the second test, 2 min elapsed before decomposition started. In the third test, 11 min elapsed. Table III lists the tests and the corresponding elapsed times. One can see that in one case decomposition started at 469 K (196 °C), before isothermal conditions could be reached, and in another case the test was terminated after 90 min because no decomposition was recorded. Repeatable results in terms of elapsed times could not be obtained using this particular method.

TABLE III.—ISOTHERMAL TGA TESTS  
PFPE F DECOMPOSITION ON  
ALPHA ALUMINA

Test run	Elapsed time, min
1	5
2	2
3	11
4	Decomposition started at 196 °C
5	8
6	Test terminated after 90 min

Another series of tests was conducted using the second heating method where the temperature was ramped 1 K/min starting at 468 K (195 °C). Table IV lists the temperatures where PFPE F started to decompose. In all cases, decomposition occurred, and it occurred over a temperature range from 471 to 483 K (198 to 210 °C). Based on these results, the second heating method was chosen to study the decomposition of PFPE F on  $\alpha$  and  $\gamma$  aluminas since decomposition would occur over the temperature range, 471 K to 483 K.

TABLE IV.—NONISOTHERMAL TGA  
TEST PFPE F DECOMPOSITION  
ON ALPHA ALUMINA

Test run	Temperature, °C
1	203
2	207
3	206
4	198
5	210
6	201

Decomposition of PFPE F proceeded slowly enough that it was possible to monitor (on the computer screen) the weight loss of the PFPE F charged alumina pellet. An entire series of tests was conducted using  $\alpha$   $\text{Al}_2\text{O}_3$  pellets in the following manner:

- (1) The TGA unit was brought up to temperature and the weight loss of the pellet was continuously monitored.
- (2) As soon as 5 percent of the initial PFPE F weight was lost, the pellet was withdrawn from the TGA and immersed in a bottle containing 3ml TCF. The resulting solution was then analyzed using HPLC.
- (3) This procedure was repeated for a 10, 20, 30, 40, 50, 60, 70, 80, and 90 percent PFPE F weight loss (the term "percent decomposed" will also be used).
- (4) The entire procedure was repeated for the  $\gamma$  alumina pellets.

For the DSC tests, the preparation and charging of the alumina pellets was identical to that of the TGA tests, and the heating method was also the same (see appendix II for DSC calibration). A charged pellet was loaded onto the sample port of the DSC chamber and an uncharged pellet was loaded onto the reference port. All tests were conducted to near complete decomposition of PFPE F.

#### TGA/HPLC Results

##### $\alpha$ -Al<sub>2</sub>O<sub>3</sub>

Figure 14 is a typical TGA thermogram of the decomposition of PFPE F on  $\alpha$ -Al<sub>2</sub>O<sub>3</sub>. This thermogram represents 90 percent decomposition of PFPE F. Decomposition started at 478 K (205 °C) and the test was

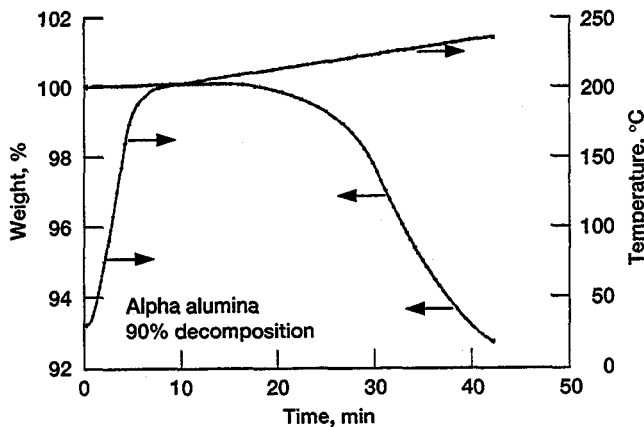


Figure 14.—TGA thermogram of 90% decomposition of PFPE F on alpha alumina.

terminated at 503 K (230 °C). Figures 15 to 18 are the HPLC chromatograms of the extracted products from  $\alpha$ - $\text{Al}_2\text{O}_3$  pellets. Table V lists the masses of the preheated pellets, the initial amount of PFPE F used, and the masses of the pellets after TCF solvent extraction and vacuum treatment.

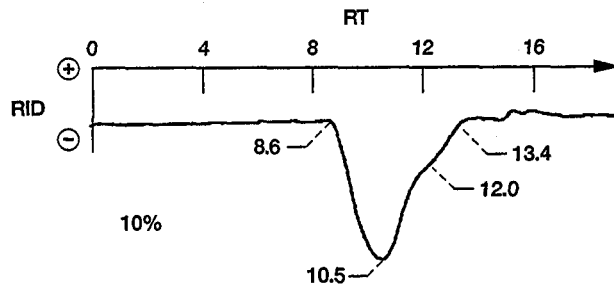
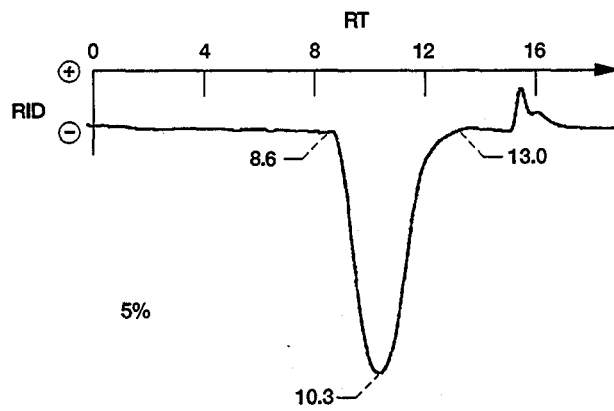
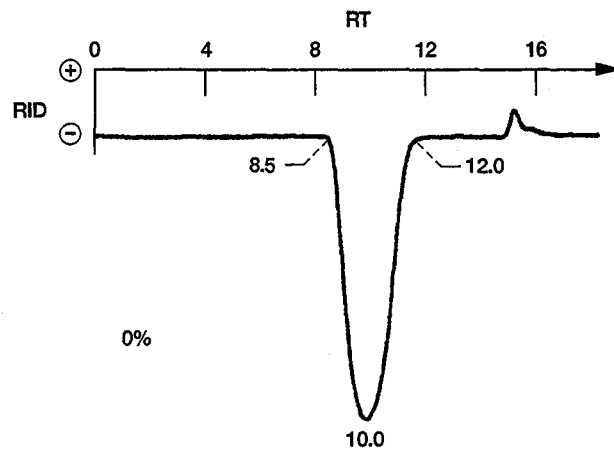
TABLE V.—ALPHA ALUMINA PELLET MASSES

Test run	Decomposition, percent	Preheated pellet mass, mg	PFPE F mass added to pellet, mg	Pellet mass after TCF extraction and vacuum, mg
1	5	53.84	4.85	54.26
2	10	51.90	4.71	52.25
3	20	51.70	3.85	51.98
4	30	50.53	4.68	50.68
5	40	52.51	4.68	52.72
6	50	55.19	4.69	55.58
7	60	54.45	4.23	54.70
8	70	54.37	4.46	54.69
9	80	55.34	4.79	55.64
10	90	53.70	4.78	53.77

Table V shows that, for the  $\alpha$ - $\text{Al}_2\text{O}_3$  runs, nearly all of the product was extracted from the pellets into the TCF solvent.

Figure 15 shows the chromatograms for the undecomposed PFPE F and for the 5 and 10 percent decomposition runs. For the 5 percent decomposition run, the presence of a lower molecular weight product (or products) is already noted by the peak tailing at 13.0 min. The peak tail for the undecomposed PFPE F terminates at 12.0 min. (see appendix I for HPLC size exclusion calibration of PFPE F). It is also noticed that the dwell peak eluted at 10.3 min compared to the 10.0-min dwell peak elution for the undecomposed PFPE F. The chromatogram for the 10 percent decomposition run reveals that the peak tailing has now extended to 13.4 min and that the dwell peak elution is now at 10.5 min. The presence of a shoulder can be seen at 12.0 min.

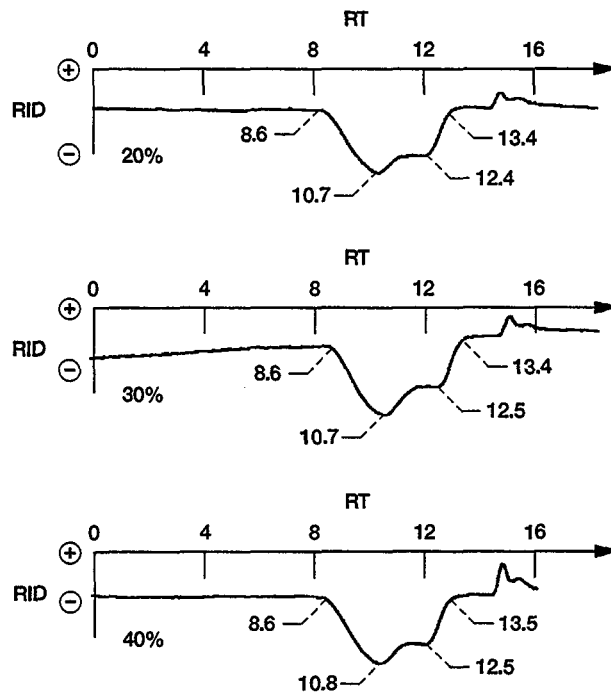
The chromatogram for the 20 percent decomposition run (fig. 16) shows the presence of a definite second dwell peak at 12.4 min. The first dwell peak has shifted to 10.7 min. The 30 and 40 percent decompositions runs (fig. 16) are similar to the 20 percent run.



Time, min	Approximate MW
10	10 200
11	6310
12	3130
13	1210
14	330

RT - Retention Time, min  
 RID - Refractive Index Detection

Figure 15.—HPLC chromatograms of 0%, 5%, and 10% decompositions, PFPE F on alpha alumina.



Time, min	Approximate MW
10	10 200
11	6310
12	3130
13	1210
14	330

RT - Retention Time, min  
 RID - Refractive Index Detection

Figure 16.—HPLC chromatograms of 20%, 30%, and 40% decompositions, PFPE F on alpha alumina.

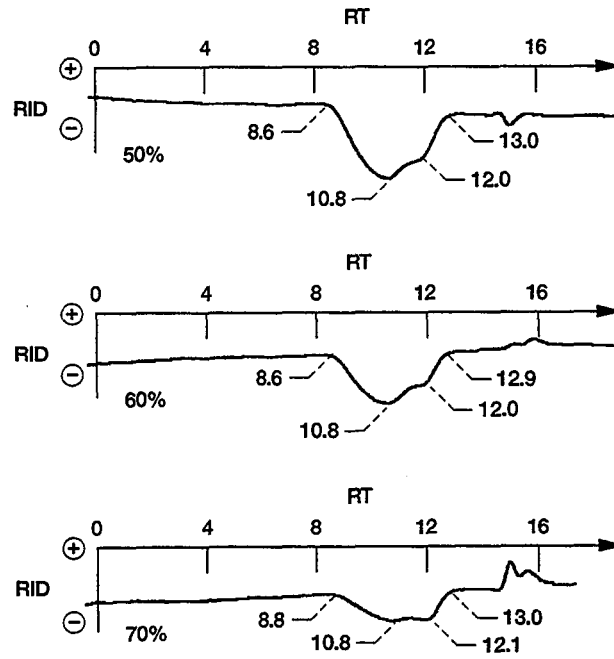
The 50 percent run (fig. 17) reveals the peak tailing terminating at 13.0 min and the second peak eluting at 12.0 min thus showing the loss of lower molecular weight product. The 60 and 70 percent runs (fig. 17) continue showing the loss of lower molecular weight product.

The 80 percent run (fig. 18) shows the peak tail terminating at 12.6 min and the absence of a definite primary and secondary peak. The chromatogram for the 90 percent decomposition run (fig. 18) shows the presence of a small amount of material beginning to elute at 8.6 min and terminating at 12.1 min. It is interesting to note that this is about the same molecular weight exclusion range as the undecomposed PFPE F.  $\gamma\text{-Al}_2\text{O}_3$

Figure 19 is a typical TGA thermogram of the decomposition of PFPE F on  $\gamma\text{-Al}_2\text{O}_3$ . This thermogram represents 90 percent decomposition of PFPE F. Figures 20 to 23 are the HPLC chromatograms of the extracted products from the  $\gamma\text{-Al}_2\text{O}_3$  pellets. Table VI, like table V, lists the various masses of pellets and amounts of PFPE F used.

TABLE VI.—GAMMA ALUMINA PELLET MASSES

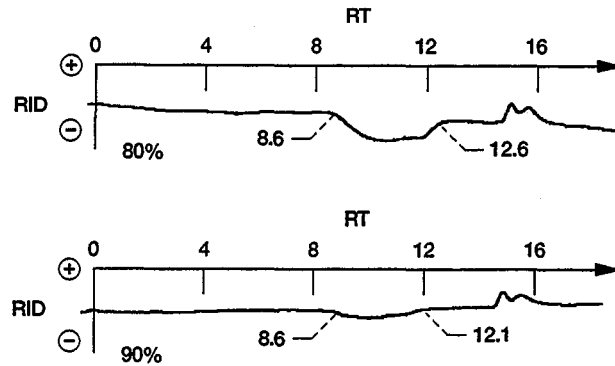
Test run	Decomposition, percent	Preheated pellet mass, mg	PFPE F mass added to pellet, mg	Pellet mass after TCF extraction and vacuum, mg
1	5	46.39	4.63	46.82
2	10	41.31	5.30	42.80
3	20	46.27	4.71	48.80
4	30	48.62	4.99	51.04
5	40	48.21	4.73	50.65
6	50	45.14	4.80	46.92
7	60	49.16	4.70	50.46
8	70	45.14	5.05	46.58
9	80	43.52	5.04	44.60
10	90	44.87	4.55	45.41



Time, min	Approximate MW
10	10 200
11	6310
12	3130
13	1210
14	330

RT - Retention Time, min  
 RID - Refractive Index Detection

Figure 17.—HPLC chromatograms of 50%, 60%, and 70% decompositions, PFPE F on alpha alumina.



Time, min	Approximate MW
10	10 200
11	6310
12	3130
13	1210
14	330

RT - Retention Time, min  
RID - Refractive Index Detection

Figure 18.—HPLC chromatograms of 80% and 90% decompositions, PFPE F on alpha alumina.

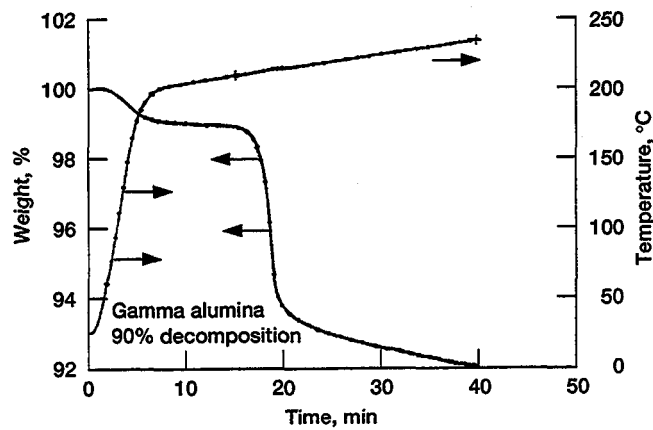


Figure 19.—TGA thermogram of 90% decomposition, PFPE F on gamma alumina.

Table VI shows that the TCF solvent was not able to dissolve and extract all the product from the pellets. In one case, more than 50 percent of the product was not extracted.

Figure 20 shows the chromatogram for the 5 and 10 percent decomposition runs. Comparison to the undecomposed PFPE F shows that, for the 5 percent run, slight formation of a lower molecular weight product has occurred as noticed by the peak tailing at 12.4 min. The 10 percent run shows the presence of lower molecular weight product due to the peak tail terminating at 12.6 min.

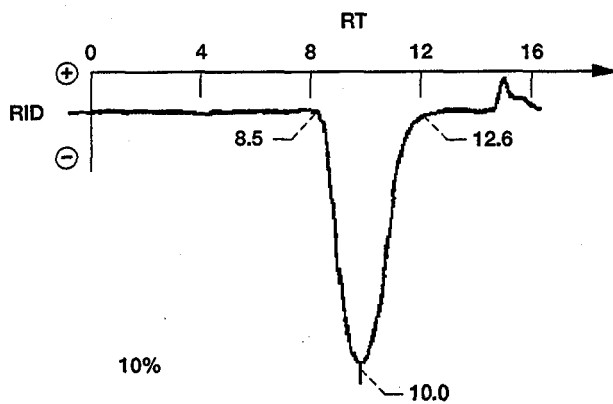
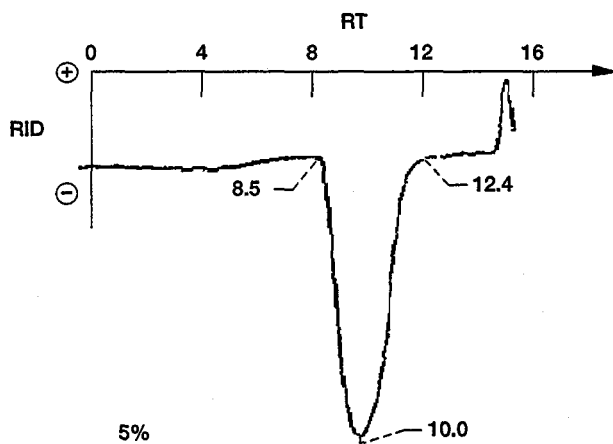
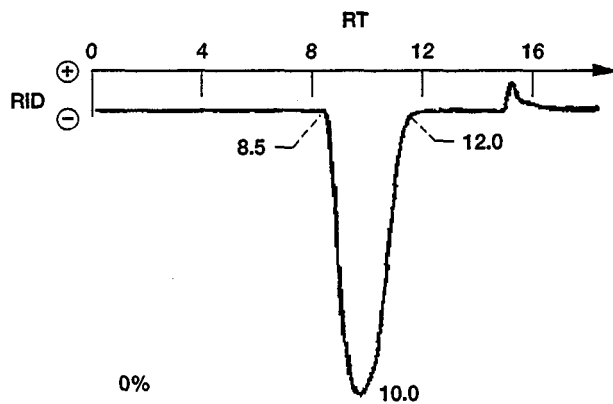
The 20 percent run (fig. 21) shows the dwell peak now eluting at 10.6 min, the presence of a shoulder at 11.8 min, and the peak tail now terminating at 13.6 min. The chromatogram for the 30 percent decomposition run (fig. 21) reveals that the product starts eluting at 9.0 min and also reveals the presence of two dwell peaks, at 11.1 and 12.3 min. The peak tail terminates at 13.8 min. The 40 percent run (fig. 21) shows product elution now starting at 9.8 min. There is only one dwell peak now at 13.0 min, and the peak tail now terminates at 14.0 min. These chromatograms indicate rapid loss of higher molecular weight material with the concomitant formation of lower molecular weight material. The 50 percent run (fig. 22) continues to show loss of the higher molecular weight material and now shows loss of the lower molecular weight material as noted by the peak tail terminating at 13.7 min. The 60 percent run (fig. 22) continues this pattern. The 70 percent run (fig. 22) reveals very little decomposition material was extracted from the pellet. A small dwell peak was detected at 12.7 min.

No peaks were detected for the 80 and 90 percent runs (fig. 23).

#### DSC Results

##### $\alpha$ -Al<sub>2</sub>O<sub>3</sub>

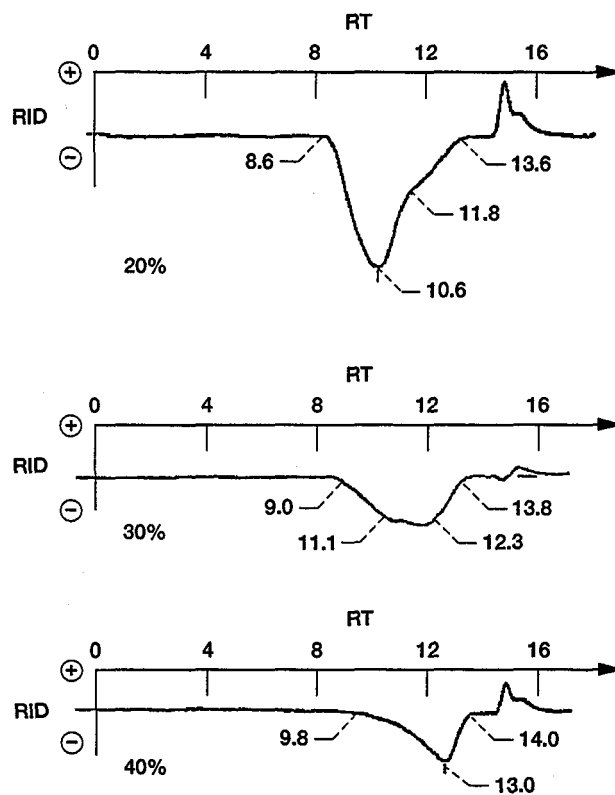
Figure 24 is the DSC thermogram of PFPE F decomposition on  $\alpha$ -Al<sub>2</sub>O<sub>3</sub> (see appendix II for DSC calibration). The thermogram shows that during the course of decomposition an initial exothermic reaction occurs, and this is followed by an endothermic reaction.



Time, min	Approximate MW
10	10 200
11	6310
12	3130
13	1210
14	330

RT - Retention Time, min  
 RID - Refractive Index Detection

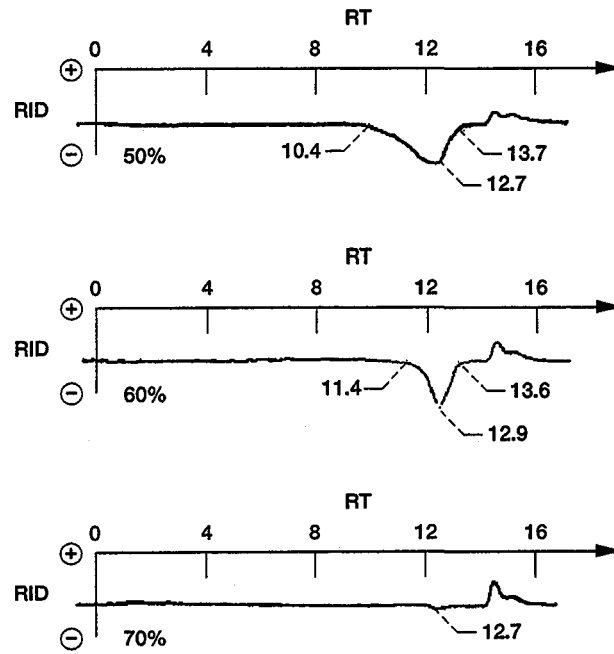
Figure 20.—HPLC chromatograms of 0%, 5%, and 10% decomposition, PFPE F on gamma alumina.



Time, min	Approximate MW
10	10 200
11	6310
12	3130
13	1210
14	330

RT - Retention Time, min  
 RID - Refractive Index Detection

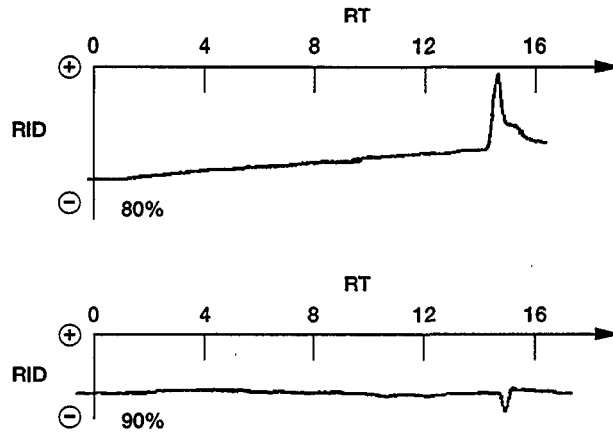
Figure 21.—HPLC chromatograms of 20%, 30%, and 40% decomposition, PFPE F on gamma alumina.



Time, min	Approximate MW
10	10 200
11	6310
12	3130
13	1210
14	330

RT - Retention Time, min  
 RID - Refractive Index Detection

Figure 22.—HPLC chromatograms of 50%, 60%, and 70% decomposition, PFPE F on gamma alumina.



Time, min	Approximate MW
10	10 200
11	6310
12	3130
13	1210
14	330

RT - Retention Time, min  
RID - Refractive Index Detection

Figure 23.—HPLC chromatograms of 80%, and 90% decomposition, PFPE F on gamma alumina.

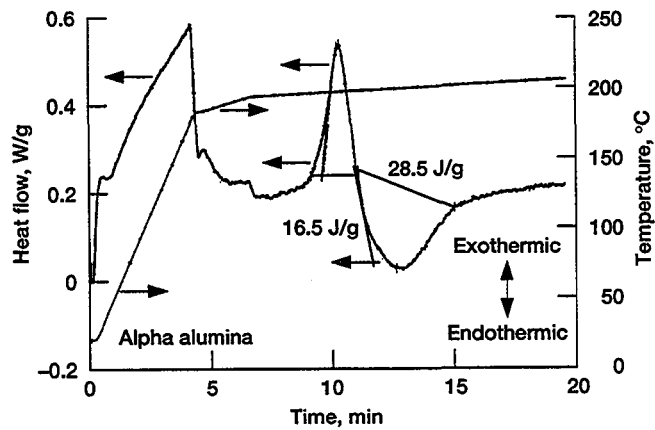


Figure 24.—DSC thermogram of PFPE F decomposition on alpha alumina.

### $\gamma$ -Al<sub>2</sub>O<sub>3</sub>

Figure 25 is the DSC thermogram of PFPE F decomposition on  $\gamma$ -Al<sub>2</sub>O<sub>3</sub>. The thermogram shows a single exothermic peak. Note that the magnitude of the heat flow axis for the  $\gamma$ -Al<sub>2</sub>O<sub>3</sub> is approximately an order-of-magnitude greater than the heat flow axis for the  $\alpha$ -Al<sub>2</sub>O<sub>3</sub>.

These two DSC thermograms were thermally analyzed by using a software program (see appendix II) that calculates the area under a peak and then normalizes it by the sample weight to determine the heat transfer, in Joules/gram, between the sample and the thermocouple. Using the initial weight of the PFPE F sample for the  $\alpha$ -Al<sub>2</sub>O<sub>3</sub> pellet, a heat transfer of 16.5 J/gr was calculated for the exothermic peak and a heat transfer of 28.5 J/gr was calculated for the endothermic peak. For the  $\gamma$ -Al<sub>2</sub>O<sub>3</sub> pellet, a heat transfer of 346.1 J/gram was calculated for the exothermic peak.

### AlF<sub>3</sub>

In addition to this DSC study using the alumina pellets, it was decided to conduct a DSC run using AlF<sub>3</sub>. AlF<sub>3</sub> powder (pellets could not be commercially obtained) was packed into a sample pan and preheated to 773 K (500 °C) under a flowing nitrogen atmosphere. The final powder weight was 21.3 mg. The AlF<sub>3</sub> powder was then charged with 4.7 mg of PFPE F and a DSC test was then performed. Figure 26 is the thermogram of this test. This thermogram is similar to the thermogram using the  $\alpha$ -Al<sub>2</sub>O<sub>3</sub> pellet where an initial exothermic peak is observed followed by an endothermic peak; however, one will notice that the reaction starts at a lower temperature of 457 K (184 °C) and terminates at 466 K (193 °C).

### Further Tests Using TGA

A saturated solution of ammonium fluoride in methanol was prepared. Preheated  $\alpha$  and  $\gamma$  alumina pellets were immersed in the solution for 24 hr (at room temperature) and then withdrawn from the solution. The pellets were then vacuum treated (<1 torr) for 1 hr. The alumina pellets were then charged with PFPE F and TGA runs were then conducted. Figure 27 is the TGA thermogram of the ammonium fluoride treated  $\alpha$  alumina pellet and figure 28 is the thermogram of the treated  $\gamma$  alumina pellet. One will notice, from the  $\alpha$  alumina thermogram, that the decomposition temperature has been extended to 533 K (260 °C). For the  $\gamma$  alumina, a

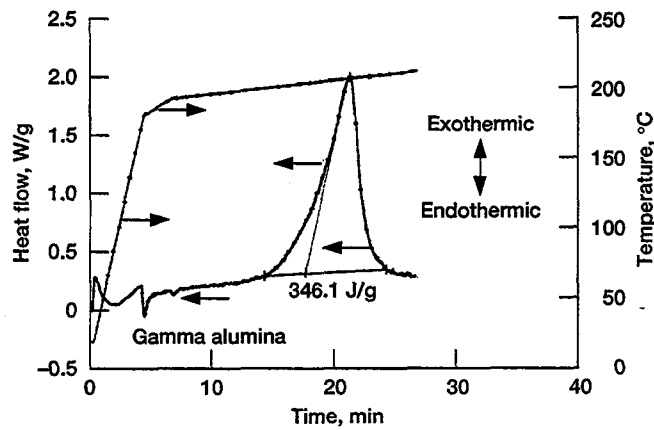


Figure 25.—DSC thermogram of PFPE F decomposition on gamma alumina.

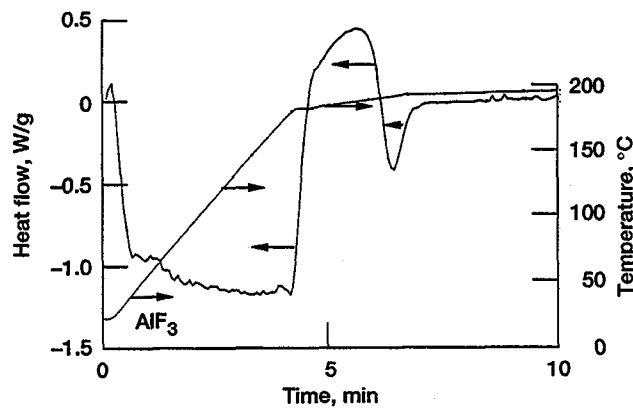


Figure 26.—DSC thermogram of PFPE F decomposition on aluminum fluoride.

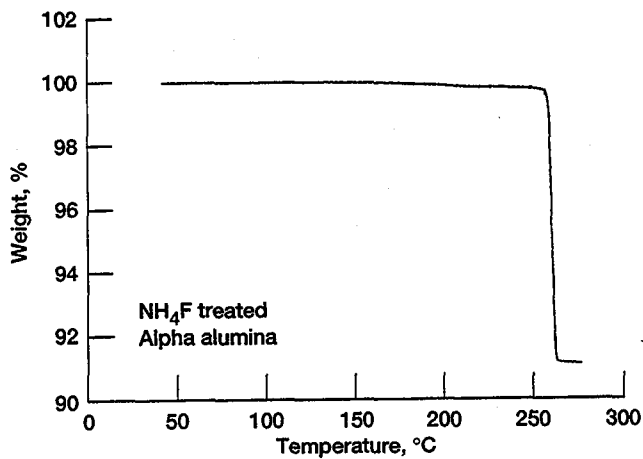


Figure 27.—TGA thermogram of PFPE F decomposition on ammonium fluoride treated alpha alumina.

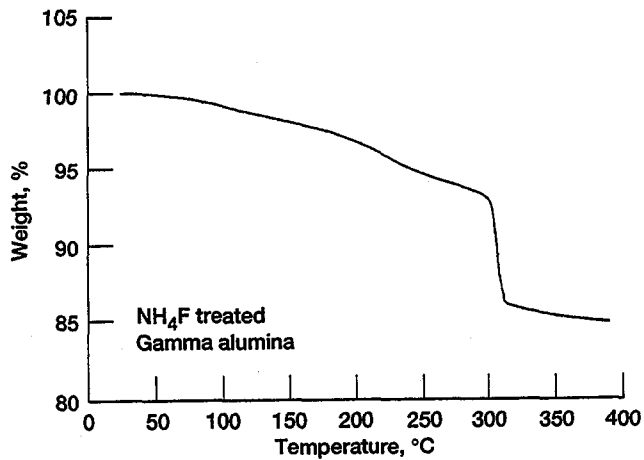


Figure 28.—TGA thermogram of PFPE F decomposition on ammonium fluoride treated gamma alumina.

steady slow decomposition is observed from 298 K (25 °C) to about 573 K (300 °C), followed by a rapid decrease in weight above 573 K.

### XPS Analysis of Aluminas

PFPE F decomposition on  $\alpha$  and  $\gamma$  alumina was carried out to 95 percent. An analysis of the alumina pellet (no extractions were made) surfaces was then performed using XPS. A MgK $\alpha$  x-ray source was used on a 1 mm spot. A pass energy of 100 eV was used for the survey spectra and 20 eV was used for the high resolution spectra. Analysis times were kept below 30 min to prevent x-ray decomposition of PFPE F on the alumina pellet surfaces. Peak identification was made in accordance with the work conducted by Herrera-Fierro, et al. (ref. 51). Herrera-Fierro, et al. vapor deposited thin films of PFPE F onto the surface of the native oxide of aluminum, clean aluminum and onto the surface of sapphire and their behavior at different temperatures was studied. XPS was used to analyze the surfaces, and chemical assignments for the spectral peaks were made. Table VII lists the XPS peak assignments as determined by Herrera-Fierro, et al.

TABLE VII.—XPS SPECTRAL FEATURES AND THEIR ASSIGNMENTS

Element	B.E., $\pm 0.2$ eV	Alpha Al <sub>2</sub> O <sub>3</sub> (-5.2 eV charging), $\pm 0.2$ eV	Gamma Al <sub>2</sub> O <sub>3</sub> (-6.7 eV charging), $\pm 0.2$ eV	Assignment
C 1s	294.7	294.7	-----	CF <sub>3</sub> or O-CF <sub>2</sub> O (PFPE F) O-CF <sub>2</sub> -CF <sub>2</sub> -O (PFPE F) C-C, aliphatic or adventitious carbon Aluminum carbide
	293.0	293.0	-----	
	284.7	-----	284.8	
	282.2	-----	-----	
O 1s	535.5	535.5	-----	PFPE F Al <sub>2</sub> O <sub>3</sub> Oxygen-compound
	532.0	531.6	532.0	
	-----	-----	530.8	
F 1s	688.7	688.6	-----	PFPE F AlF <sub>3</sub> Al-oxyfluoride
	687.2	-----	-----	
	685.1	684.8	685.1	
Al 2p	73.0	-----	-----	Al <sup>0</sup> Al-carbide Al-oxide Al-fluoride AlF <sub>6</sub> <sup>3-</sup>
	73.7	-----	-----	
	75.1	75.1	74.3	
	76.6	-----	-----	
	78.0	-----	-----	

Figure 29 is the XPS survey spectrum of the  $\alpha$  alumina surface. Before the peaks could be identified, 5.2 eV had to be subtracted from all peaks. This was done in order to account for the charging of the  $\alpha$

alumina. Figures 30 and 31 show the high resolution spectra of the peaks of interest—C 1s, F 1s, and O 1s, Al 2p. For the XPS C 1s spectrum (fig. 30(a)), the binding energies from 298.2 to 299.9 eV are assigned to the carbons in PFPE F. There appears to be a trace of hydrocarbon contaminant at about 290 to 292 eV. For the F 1s spectrum (fig. 30(b)), the binding energy at 693.9 eV is assigned to the fluorine in PFPE F. There appears to be a trace of Al-oxyfluoride at about 690 eV. For the O 1s spectrum (fig. 31(a)), the binding energy at 540.7 eV is assigned to the oxygen in PFPE F whereas the binding energy at 536.8 eV is assigned to  $Al_2O_3$ . For the Al 2p spectrum (fig. 31(b)), the binding energy at 80.3 eV is assigned to an aluminum oxide.

Figure 32 is the XPS survey spectrum of the  $\gamma$  alumina surface. The charging of the  $\gamma$  alumina was 6.7 eV. For the C 1s spectrum (fig. 33(a)), the binding energy at 291.5 eV is assigned to adventitious carbon. For the F 1s spectrum (fig. 33(b)), the binding energy at 691.8 eV is assigned to an Al-oxyfluoride. For the O 1s spectrum (fig. 34(a)), the binding energy at 537.5 eV is assigned to an unknown oxygen compound. There appears to be shoulder at 538.7 eV which is assigned to  $Al_2O_3$ . For the Al 2p spectrum (fig. 34(b)), the binding energy at 81.0 eV appears to be midway between Al-carbide and Al-oxide.

#### Discussion of Thermal, HPLC, and XPS Data

Analysis of the TGA and DSC thermograms reveals that the decomposition of PFPE F on  $\alpha$  alumina is different from the decomposition on  $\gamma$  alumina. The HPLC chromatograms also support evidence for the existence of two different decomposition pathways. In addition, XPS analysis of the  $\alpha$  and  $\gamma$  alumina surfaces, at the end of 95 percent PFPE F decomposition runs, reveals the presence of different surface species.

#### TGA

Comparison between the 90 percent decomposition TGA thermograms (figs. 14 and 19) shows that for the  $\alpha$  alumina no weight loss is observed until the temperature reaches 478 K (205 °C), and this is followed by a slow decrease in weight; for the  $\gamma$  alumina a small decrease in weight ( $\approx 1$  percent) is observed between room temperature and 481 K (208 °C), this is followed by a rapid decrease in weight between 481 K and 485 K, and then this is followed by a slow decrease in weight between 485 K and 507 K. This comparison suggests that, for the  $\alpha$  alumina, the decomposition pathway involves no interaction between PFPE F and the  $\alpha$  alumina

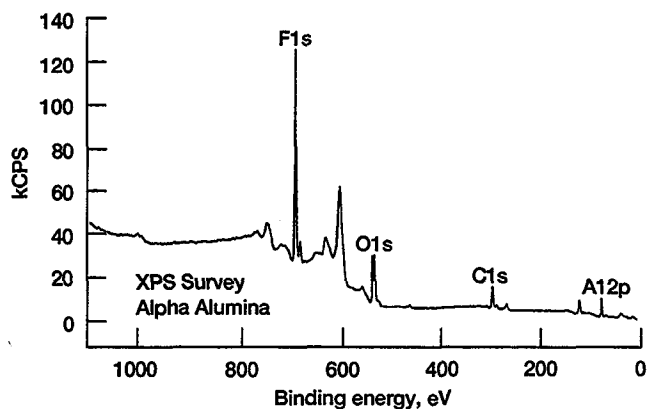


Figure 29.—XPS survey spectrum of used alpha alumina surface.

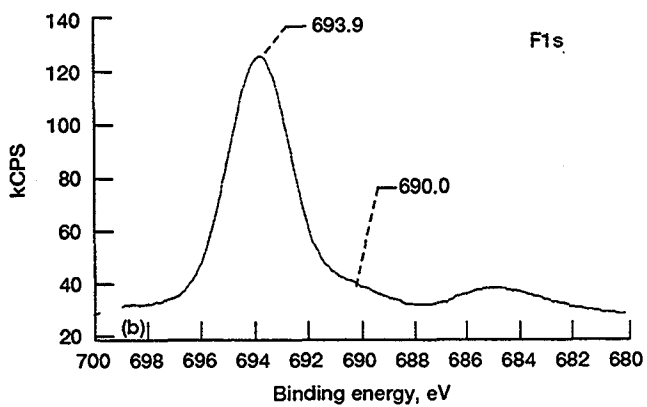
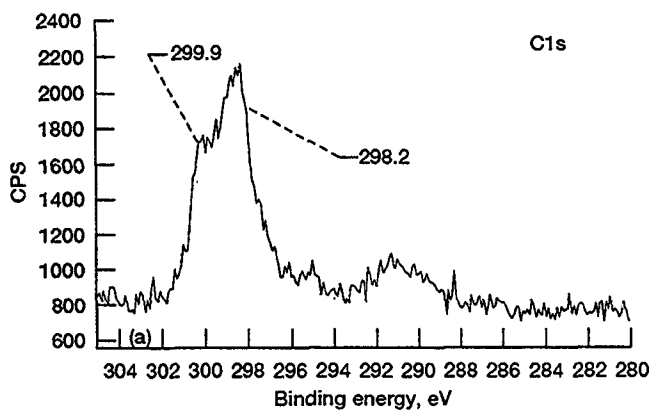


Figure 30.—Enhanced XPS spectra of (a) C1s peak, and (b) F1s peak. For used alpha alumina surface.

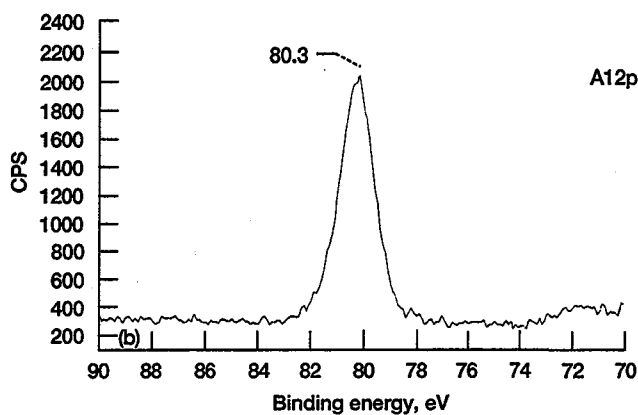
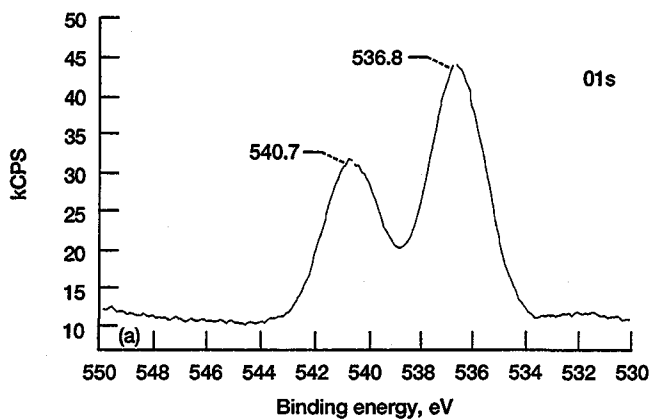


Figure 31.—Enhanced XPS spectra of (a) O1s peak, and (b) Al2p peak. For used alpha alumina surface.

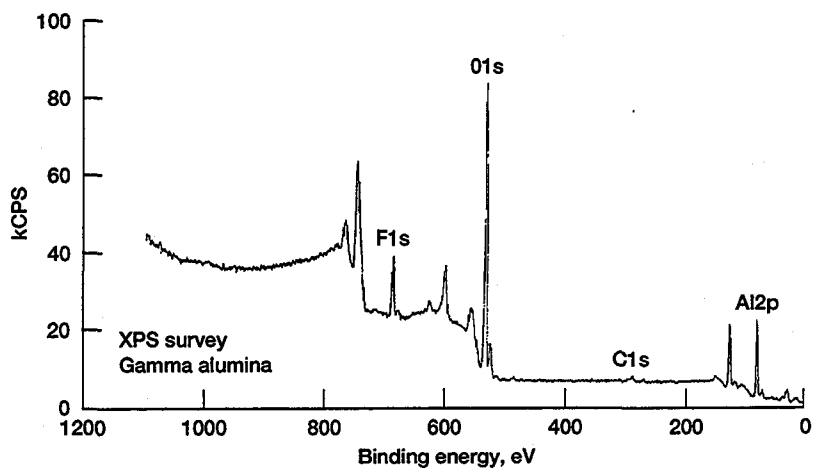


Figure 32.—XPS survey spectrum of used gamma alumina surface.

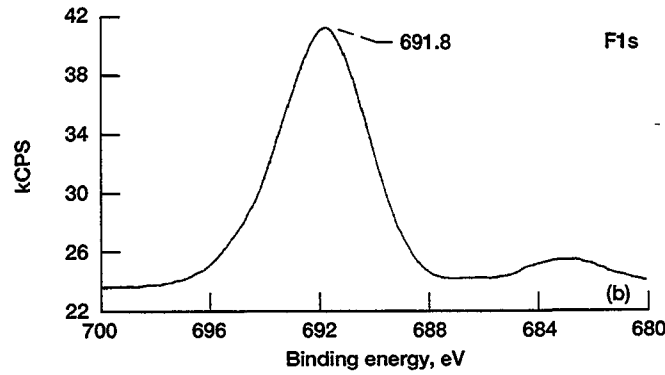
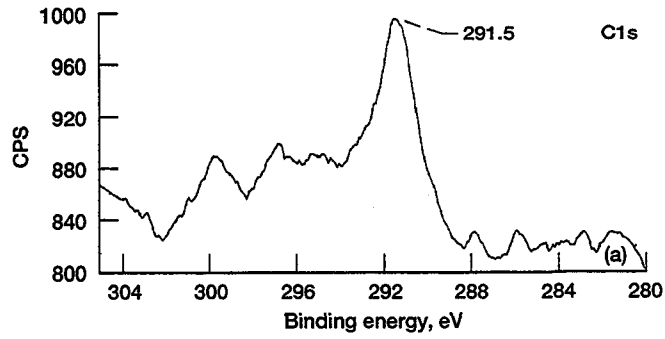


Figure 33.—Enhanced XPS spectra of (a) C1s peak, and (b) F1s peak. For used gamma alumina surface.

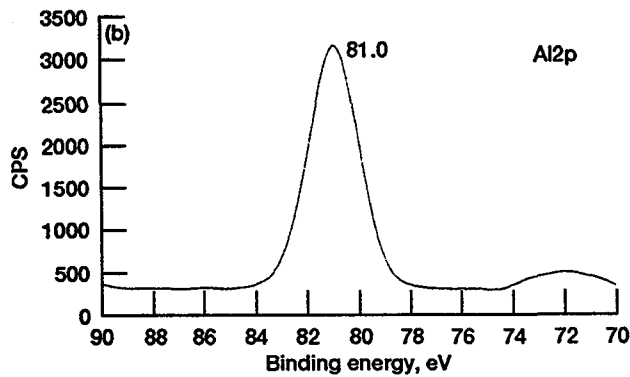
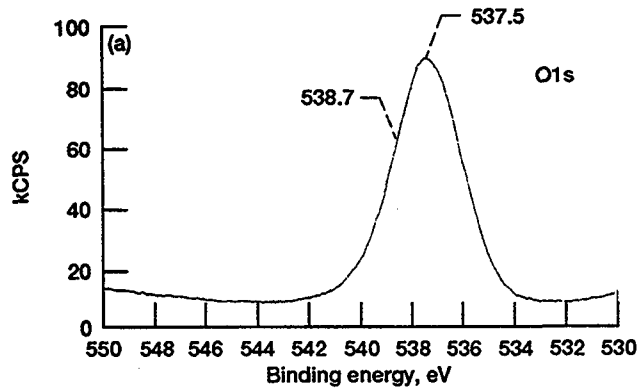


Figure 34.—Enhanced XPS spectra. (a) O1s peak. (b) Al2p peak. For used gamma alumina surface.

surface until a critical temperature (in this case 478 K) is reached where upon a slow decomposition occurs; for the  $\gamma$  alumina the decomposition pathway involves an initial interaction between PFPE F and the  $\gamma$  alumina surface from room temperature to a critical temperature (in this case 481 K) where upon a rapid decomposition reaction occurs and this is followed by a slow weight loss.

### HPLC

Analysis of the HPLC chromatograms reveals several things. For the  $\alpha$  alumina 5 percent decomposition run (fig. 15), moderate changes in the molecular size distribution can already be detected by the shift of the dwell peak from 10.0 to 10.3 min and the appearance of smaller molecular weight product down to 13.0 min. Subsequent analysis of the HPLC chromatograms shows a gradual decrease of the higher molecular weight material relative to the formation of lower molecular weight product (figs. 16 and 17) up to 40 percent decomposition. From 50 to 90 percent decomposition (figs. 17 and 18), a gradual decrease of both higher and lower molecular weight product was observed.

For the  $\gamma$  alumina 5 percent decomposition run (fig. 20), slight formation of a lower molecular weight product was observed. Subsequent analysis of the HPLC chromatograms shows that abrupt changes occurred between the 10 and 30 percent decomposition runs (fig. 21) where the formation of lower molecular weight product was accompanied by the rapid decrease of higher molecular product. Between the 40 and 70 percent runs (figs. 21 and 22), a gradual decrease of all extracted product down to a single peak, having an approximate molecular weight of 1000, was observed.

### XPS

XPS analysis of the  $\alpha$  alumina surface, at the end of a 95 percent decomposition run, reveals the presence of two main species, PFPE F and  $\text{Al}_2\text{O}_3$ . For the  $\gamma$  alumina surface, XPS analysis also reveals the presence of two main species,  $\text{Al}_2\text{O}_3$ , and an Al-oxyfluoride.

The thermal, HPLC, and XPS data suggest that PFPE F decomposition on  $\alpha$  alumina proceeds in a two step process where, at a critical activation temperature, an initial exothermic scission of the molecules occurs followed by endothermic depolymerization of the scissioned fragments. The data for PFPE F decomposition on

$\gamma$  alumina suggest an initial reaction occurs between PFPE F and the  $\gamma$  alumina surface starting at room temperature and up to a critical temperature. At the critical temperature a rapid exothermic reaction occurs. This reaction leads to the formation of lower molecular weight products, soluble in TCF solvent, and an insoluble product (Al-oxyfluoride). As the temperature increases, the lower molecular weight products either decompose or vaporize, and the insoluble product thermally desorbs or decomposes.

If, as has been suggested by several authors, PFPE F decomposition on certain metal oxides proceeds via initial fluorination of the metal oxide surface to a metal fluoride followed by a Lewis acid catalytic attack on the PFPE F molecules, then PFPE F decomposition on  $\text{AlF}_3$  should be a one step process. The DSC thermogram (fig. 26) shows that  $\text{AlF}_3$  behaves very similar to  $\alpha$  alumina, in that, an initial exothermic reaction occurs followed by an endothermic reaction—a two-step decomposition mechanism.

#### $\text{NH}_4\text{F}$ Treatment

Fluorine incorporated into oxide catalysts enhances the acidity of Lewis acid sites on the surface (ref. 53). If Lewis acid sites are responsible for PFPE F decomposition, then fluorine incorporation into  $\alpha$  and  $\gamma$  alumina should lead to lower decomposition temperatures. The TGA thermogram (fig. 27) for fluorine treated  $\alpha$  alumina shows PFPE F decomposition starting to occur at 529 K (256 °C). The TGA thermogram (fig. 28) for fluorine treated  $\gamma$  alumina shows a gradual decomposition of PFPE F with increasing temperature until 573 K (300 °C) is reached and then rapid decomposition occurs.

Flockhart et al. (ref. 54) studied the electron donor properties of an alumina surface and was able to associate the electron donor sites with surface hydroxyl ions and with intrinsic oxide ion defect centers. They published a series of subsequent papers but one in particular stands out. In 1974 Flockhart et al. (ref. 55) carried out the reduction of iodine on an alumina surface, and then they showed that incorporation of fluorine into the alumina resulted in substantial lowering of the reducing activity of the alumina.

The thermal and HPLC analysis of these decomposition experiments support the view that reducing sites, on alumina, are responsible for PFPE F decomposition. The nature of these reducing sites are different for  $\alpha$  and  $\gamma$  alumina as evidenced by the two different reaction paths. Since the DSC thermograms of PFPE F

decomposition on  $\alpha$  alumina and  $AlF_3$  are similar, it can be concluded that the active reducing sites on  $\alpha$  alumina and  $AlF_3$  are the same. These reducing sites can be hydroxyl groups. On the other hand, the active reducing sites on  $\gamma$  alumina are speculated to be the oxide ion defect sites. This contention is supported by the fact that  $\gamma$  alumina has an inherent defect spinal structure with a deficit of cations and upon removal of water and hydroxyl groups unsaturated oxygen ions, and  $Al^{3+}$  cations, are created (ref. 54). The work by Basu et al. (ref. 46) also supports this speculation by showing evidence that an "oxygen center" was responsible for the decomposition of a fluoro-ether on  $\gamma$  alumina.

### INHIBITING PFPE F DECOMPOSITION

Since the analysis of the thermal experiments shows evidence that different reducing sites on  $\alpha$  and  $\gamma$  alumina are responsible for PFPE F decomposition, a means was sought to effectively deactivate these sites. A review of the work of Flockhart et al. (ref. 55) revealed that the incorporation of small quantities of silica into alumina resulted in substantial lowering of the activity of the reducing sites. After a review of the commercially available silicon containing compounds, three compounds were chosen to be tested as deactivators. These compounds were chosen because they were liquid (at room temperature), easy to handle without special precautions, and relatively nontoxic. Figure 35 gives the names and structures of the three compounds.

1.  $(CH_3)_2 Si(OC_2H_5)_2$  bp 114 °C  
Diethoxydimethylsilane
2.  $(CH_3)_2 NSi(CH_3)_3$  bp 86 °C  
Dimethylaminotrimethylsilane
3.  $NH_2 (C_3H_6) Si(OC_2H_5)_3$  bp 217 °C  
3-Aminopropytriethoxysilane

Figure 35.—Chemical formulas of test silanes.

Preheated  $\alpha$  and  $\gamma$  alumina pellets were immersed in a beaker containing 5 ml of silane 1 for 2 hr. The pellets were withdrawn from the beaker and stored under vacuum ( $<1$  torr) for 30 min at room temperature. The pellets were then placed inside the TGA unit and heated to 393 K (120 °C) (6 K above the boiling temperature of silane 1). After the TGA unit cooled down back to room temperature, the pellets were charged with PFPE F and TGA test runs were then conducted. This procedure was also used for silane 2, except that the pellets were heated, inside the TGA unit, to 373 K (100 °C) (14 K above the boiling temperature of silane 2) before charging the pellets with PFPE F. Table VIII lists the masses of the pellets during the various stages of silane 1 and 2 treatment, the amount of PFPE F used, and the pellet masses at the end of the TGA tests.

TABLE VIII.—ALUMINA PELLET MASSES SILANE TREATMENT

Silane	Pellet type	Preheated pellet mass, mg	Pellet mass after silane treatment, mg	PFPE F mass added to pellet, mg	Pellet mass at test end, mg
1	Alpha	52.98	53.31	4.73	53.08
	Gamma	48.11	48.99	5.01	48.13
2	Alpha	54.89	54.99	4.57	54.99
	Gamma	46.71	46.89	4.74	46.80
3	Alpha	51.13	51.73	4.80	55.30
	Gamma	47.97	49.10	4.85	48.31

A different method for impregnating the alumina pellets with silane 3 was used due to the high viscosity of silane 3. Immersing and then withdrawing the pellets from silane 3 results in the formation of a thick oily coating, about the entire pellets, which could not be removed by evacuation. A solution of silane 3 in methanol was prepared by dissolving 100 mg of silane 3 in 5 ml of methanol. The alumina pellets were then immersed in this solution for 2 hr, withdrawn and then vacuum treated. After vacuum treatment, the pellets were placed in the TGA unit and heated to 489 K (225 °C) (8 K above the boiling point of silane 3). The pellets were then charged with PFPE F, after the TGA unit cooled down to room temperature, and TGA test runs were then conducted. All pellet masses during the various stages of silane 3 treatment, and the amount of PFPE F used are listed in table VIII.

Figures 36 and 37 are the TGA thermograms for silane 1 treatment. PFPE F decomposition on  $\alpha$  alumina (fig. 36) now occurred at about 573 K (300 °C). For  $\gamma$  alumina (fig. 37) it can be seen that a small weight loss ( $\approx 1$  percent) occurred between room temperature and 573 K, and this was followed by a rapid decomposition of PFPE F at 573 K.

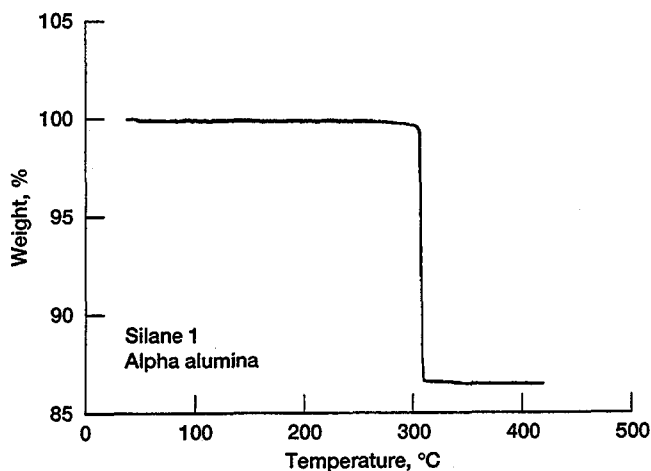


Figure 36.—TGA thermogram of PFPE F decomposition on silane 1 treated alpha alumina.

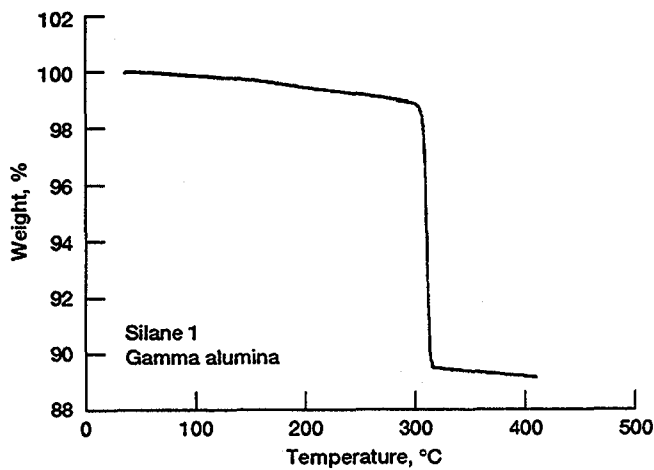


Figure 37.—TGA thermogram of PFPE F decomposition on silane 1 treated gamma alumina.

Figures 38 and 39 are the TGA thermograms for silane 2 treatment. PFPE F decomposition on  $\alpha$  alumina (fig. 38) now occurred at about 523 K (250 °C). For  $\gamma$  alumina (fig. 39) a small weight loss ( $\approx 1$  percent) occurred between room temperature and 553 K (280 °C), and this was followed by rapid decomposition of PFPE F at 553 K.

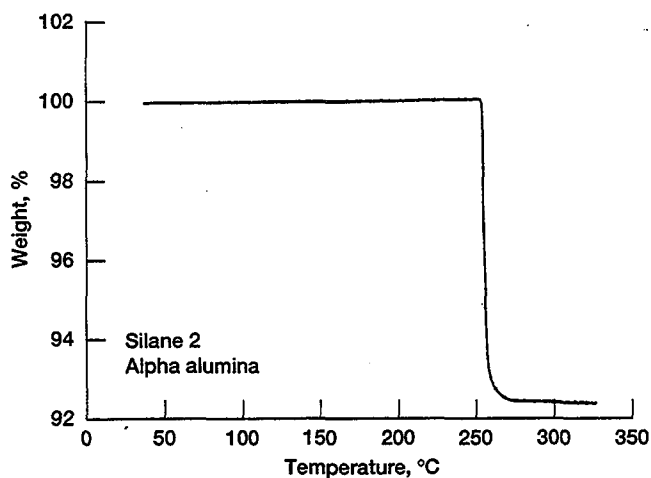


Figure 38.—TGA thermogram of PFPE F decomposition on silane 2 treated alpha alumina.

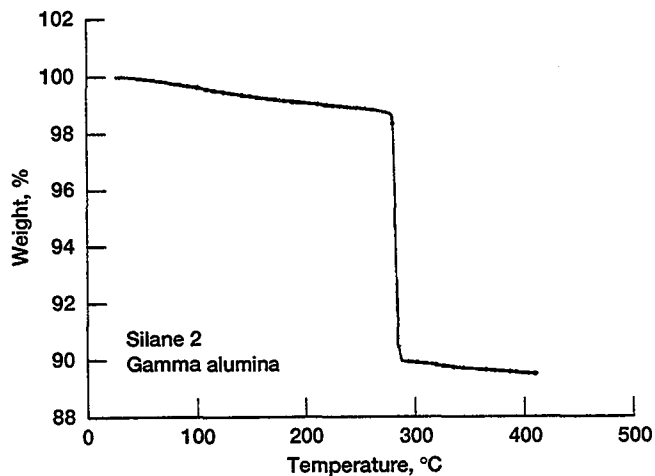


Figure 39.—TGA thermogram of PFPE F decomposition on silane 2 treated gamma alumina.

Figures 40 and 41 are the TGA thermograms for silane 3 treatment. For the  $\alpha$  alumina pellet (fig. 40) only a weight loss of about 2.5 percent was recorded up to a temperature of 673 K (400 °C) where the test was terminated. For the  $\gamma$  alumina (fig. 41) rapid decomposition of PFPE F now occurred at about 648 K (375 °C).

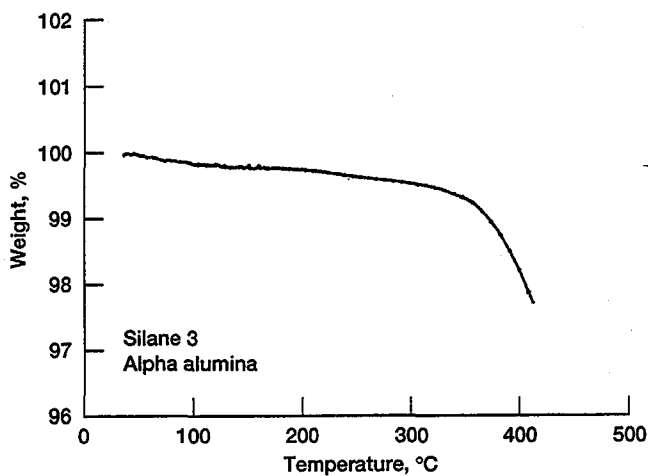


Figure 40.—TGA thermogram of PFPE F decomposition on silane 3 treated alpha alumina.

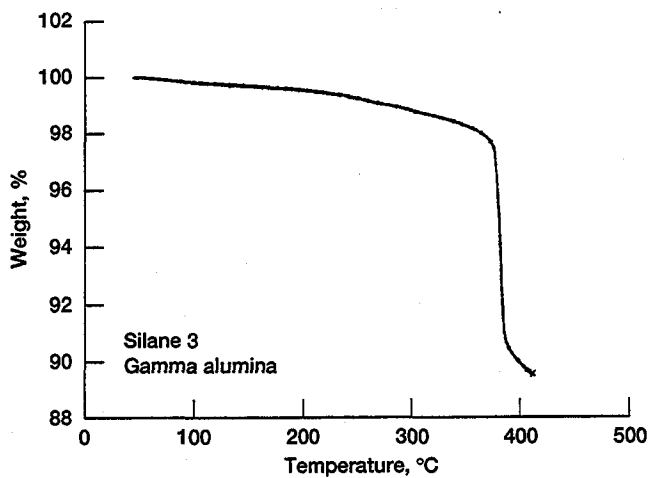


Figure 41.—TGA thermogram of PFPE F decomposition on silane 3 treated gamma alumina.

In all cases, silane treatment has been shown to inhibit PFPE F decomposition on both  $\alpha$  and  $\gamma$  aluminas until higher temperatures ( $>523$  K) have been reached.

#### MICRO-OXIDATION TEST REVISITED

Since silane 3 has been shown to inhibit PFPE F decomposition on  $\alpha$  and  $\gamma$  alumina above 618 K (345 °C), it was decided to use silane 3 in conjunction with the Penn State Micro-Oxidation Test. A solution was prepared by dissolving 1 ml of silane 3 in 20 ml of methanol. A 440C SS catalyst specimen was then immersed in the solution for 1 min, withdrawn from the solution and placed on a hot plate (at 498 K) for 1 min. The 440C SS catalyst specimen was then placed inside the micro-oxidation glassware under a flowing nitrogen atmosphere. After a 10-min waiting period, the catalyst specimen was charged with 50  $\mu$ l of PFPE F and a 30-min micro-oxidation test was conducted at 618 K under a flowing air atmosphere. At test conclusion, 5 ml of TCF solvent was used to dissolve any remaining PFPE F on the surface of the 440C SS catalyst specimen. Figure 42(a) is the HPLC chromatogram of the TCF extract. Comparison with the HPLC chromatogram of unused PFPE F (fig. 42(b)) revealed no decomposition occurred, unlike the original micro-oxidation test where total decomposition occurred (fig. 4).

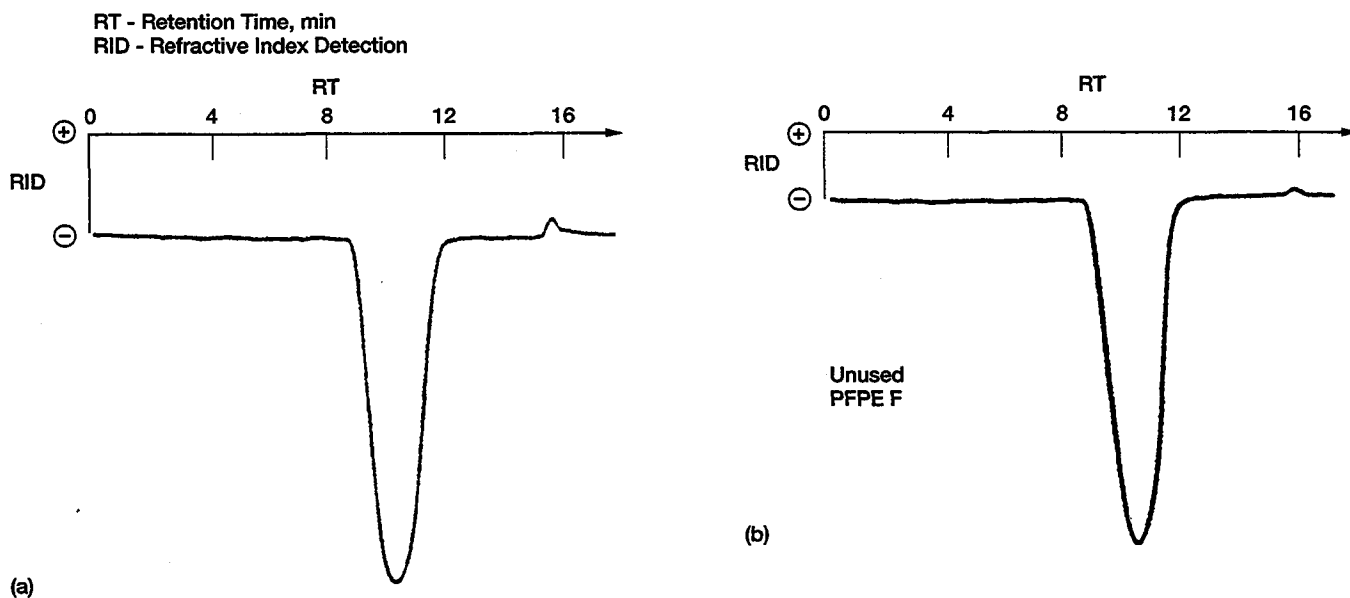


Figure 42.—(a) HPLC chromatogram of PFPE F remaining on surface of silane 3 treated 440C SS under air atmosphere, 345 °C. (b) HPLC chromatogram of unused PFPE F.

## CONCLUSIONS

Although much information about PFPE F decomposition was obtained using the Penn State Micro-oxidation Test apparatus, several drawbacks (high test temperature and lack of repeatable decomposition runs) led to the use of a TGA/DSC thermal unit employing catalyst alumina pellets. It was found that PFPE F decomposition could be studied at lower temperatures ( $\approx 473$  K for the TGA/DSC unit versus 618 K for the micro-oxidation apparatus), and under conditions that led to repeatable results.

It was concluded, based on the analysis of the TGA/DSC experimental data, HPLC and XPS data, that PFPE F decomposition on  $\alpha$  alumina was different from decomposition on  $\gamma$  alumina. It was also concluded that reductive sites (on both aluminas), and not Lewis acid sites, were responsible for PFPE F decomposition. Treatment of both aluminas with three different liquid silanes led to the inhibition of PFPE F decomposition. Surface treatment of a 440C SS catalyst specimen with silane 3 completely inhibited the decomposition of PFPE F, at 618 K in an air atmosphere, using the Penn State Micro-oxidation Test. It is believed that this surface treatment silylated the metal surface and this deactivated the catalytic sites.

## REFERENCES

1. Gumprecht, W.H.: PR-143—A New Class of High Temperature Fluids. ASLE Trans., 9, 1966, pp. 24-30.
2. Sianesi, D.: Chim. Ind. (Milan) 50, 1968, p. 206.
3. Holland, L.; Laurenson, L.; and Baker, P.N.: Vacuum 1972, 22, p. 315.
4. Hennings, J.; and Lutz, H.: Vacuum 1977, 27, p. 171.
5. Luches, A.; and Provenzano, I.: J. Phys. D: Appl. Phys. 1977, 10, p. 339.
6. Sianesi, D.; Zamboni, V.; Fontanelli, R.; and Binaghi, M.: Wear 1971, 18, p. 85.
7. Cantow, M.J.R.; Larrabee, R.B.; Barrall II, E.M.; Butner, R.S.; Cotts, P.; Levy, F.; and Ting, T.Y.:  
Molecular Weights and Molecular Dimensions of Perfluoropolyether Fluids. Makromol. Chem. 187, 1986,  
pp. 2475-2481.
8. Ouano, A.C.; and Appelt, B.: Poly(Perfluoroethers): Viscosity, Density and Molecular Weight Relationships.  
ACS Polymer Science Proc., Vol. 46, pp. 230-236.

9. Cantow, M.J.R.; Barrall II, E.M.; Wolf, B.A.; and Geerissen, H.: Temperature and Pressure Dependence of the Viscosities of Perfluoropolyether Fluids. *J. Poly. Sci.: Part B: Polymer Physics*, Vol. 25, 1987, pp. 603–609.
10. Pacansky, J.; Miller, M.; Hatton, W.; Liu, B.; and Scheiner, A.: Study of the Structure of Perfluoro Ethers. *J. Am. Chem. Soc.*, 1991, 113, pp. 329–343.
11. Jones, W.R., Jr.; Paciorek, K.J.L.; Ito, T.I.; and Kratzer, R.H.: Thermal Oxidative Degradation Reactions of Linear Perfluoroalkyl Ethers. I and EC Product Research and Development, Vol. 22, June 1983, pp. 166–170.
12. Helmick, L.S.; and Jones, W.R., Jr.: Determination of the Thermal Stability of Perfluoroalkylethers by Tensimetry. NASA TM–102116.
13. Smart, B.E.; and Dixon, D.A.: Heterolytic C–F Bond Energies and Stabilities of Poly(Perfluoroethers). *J. Fluor. Chem.*, 57, 1992, pp. 251–258.
14. Walczak, M.M.; Leavitt, P.K.; and Thiel, P.A.: Oxygenated Fluorocarbons Adsorbed at Metal Surfaces. *J. Am. Chem. Soc.*, 1987, 109, pp. 5621–5627.
15. Napier, M.E.; and Stair, P.C.: Decomposition Pathway for Model Fluorinated Ethers on the Clean Iron Surface. *J. Vac. Sci. Technol. A* 10(4), Jul./Aug. 1992.
16. Herrera-Fierro, P.C.; Jones, W.R., Jr.; and Pepper, S.V.: Interfacial Chemistry of a Perfluoropolyether Lubricant Studied by XPS and TDS. NASA TM–105840, Oct. 1992.
17. Pacansky, J.; Waltman, R.J.; and Wang, C.: Irradiation of Poly(Perfluoropropylene Oxide) by a 175 KV Electron Beam. *J. Fluor. Chem.*, 32, 1986, pp. 283–297.
18. D'Anna, E.; Leggieri, G.; Luches, A.; and Perrone, A.: Fragmentation Spectra and Appearance Potentials of Vacuum Pump Fluids Determined by Electron Impact Mass Spectrometry. *J. Vac. Sci. Technol. A* 5(6), Nov./Dec. 1987.
19. Pacansky, J.; and Waltman, R.J.: Electron Beam Irradiation of Poly(Perfluoro ethers). *J. Phys. Chem.*, 1991, 95, pp. 1512–1518.

20. Ohtani, H.; Lin, J.; and Seki, H.: The Response of Perfluoropolyether Thin Films on Au to UV Irradiation. Proceedings of the Japan International Tribology Conference, Nagoya, 1990.
21. Saperstein, D.D.; and Lin, L.J.: Improved Surface Adhesion and Coverage of Perfluoropolyether Lubricants Following Far-UV Irradiation. *Langmuir*, Vol. 6, No. 9, 1990.
22. Vurens, G.H.; Gudeman, C.S.; Lin, L.J.; and Foster, J.S.: Mechanism of UV and Electron Bonding of Perfluoropolyethers. *Langmuir*, Vol. 8, No. 4, 1992.
23. Mori, S.; and Morales, W.: Degradation and Crosslinking of Perfluoroalkyl Polyethers. NASA TP-2910, 1989.
24. Mori, S.; and Morales, W.: X-ray Photoelectron Spectroscopy Peak Assignment for Perfluoropolyether Oils. *J. Vac. Sci. Technol. A* 8(4), Jul./Aug. 1990.
25. Sianesi, D.; Zamboni, V.; Fontanelli, R.; and Binaghi, M.: Perfluoropolyethers: Their Physical Properties and Behaviour at High and Low Temperatures. *Wear*, 18, 1971, pp. 85-100.
26. Snyder, C.E., Jr.; Gschwender, L.J.; and Tamborski, C.: Linear Polyperfluoroalkylether-Based Wide-Liquid-Range High-Temperature Fluids and Lubricants. *Lubrication Engineering*, Vol. 37, 6, 1980, pp. 344-349.
27. Jones, W.R., Jr.; and Snyder, C.E., Jr.: Boundary Lubrication, Thermal and Oxidative Stability of a Fluorinated Polyether and a Perfluoropolyether Triazine. *ASLE Trans.*, Vol. 23, 3, pp. 253-261.
28. Cosmacini, E.; and Veronesi, V.: A Study of the Tribological Behaviour of Perfluoropolyethers. *Wear*, 108, 1986, pp. 269-283.
29. Morales, W.; and Buckley, D.H.: Concentrated Contact Sliding Friction and Wear Behaviour of Several Ceramics Lubricated With a Perfluoropolyalkylether at 25 °C. *Wear*, 123, 1988, pp. 345-354.
30. D'Agostino, V.; Niola, V.; and Caporiccio, G.: Tribological Behaviour of Sintered Iron Bearings Self-Lubricated With PFPE. *Tribology International*, Vol. 21, No. 2, Apr 1988.
31. Moulder, J.F.; Hammond, J.S.; and Smith, K.L.: Using Angle Resolved ESCA to Characterize Winchester Disks. *Appl. Surf. Sci.*, 25, 1986, pp. 446-454.

32. Anderson, J.C.; Flabbi, L.; and Caporiccio, G.: The Lubrication of Plastics by Perfluoropolyether Fluids. *J. Syn. Lubri.*, 5-3, pp. 199-214.
33. Conley, P.; and Bohner, J.: Experience with Synthetic Fluorinated Fluid Lubricants. 24th Aerospace Mechanisms Symposium, NASA CP-3062, 1990, p. 213.
34. Watson, N.D.; Miller, J.B.; Taylor, L.V.; Lovell, J.B.; Cox, J.W.; Fedors, J.C.; Kopia, L.P.; Holloway, R.M.; and Bradley, O.H.: Earth Radiation Budget Experiment (ERBE) Scanner Instrument Anomaly Investigation. NASA TM-87636, Oct. 1985.
35. Mori, S.; and Morales, W.: Decomposition of PFPE in Ultra-High Vacuum Under Sliding Conditions. *Trib. Trans.*, Vol. 33, 3, 1990, pp. 325-332.
36. Mori, S.; and Morales, W.: Tribological Reactions of PFPE Oils with Stainless Steel Under Ultrahigh Vacuum Conditions. *Wear*, 132, 1989, pp. 111-121.
37. Masuko, M; Fujinami, I.; and Okabe, H.: Lubrication Performance of Perfluoropolyalkylethers Under High Vacuum. *Wear*, 159, 1992, pp. 249-256.
38. Shubking, R.L., ed.: *Synthetic Lubricants and High-Performance Functional Fluids (Book)*; Chap. 6, Marcel Dekker, Inc. 1993, pp. 154-155.
39. Shubking, R.L., ed.: *Synthetic Lubricants and High-Performance Functional Fluids (Book)*; Chap. 6, p. 159, Marcel Dekker, Inc. 1993.
40. Van Dyke Tiers, G.: The Chemistry of Perfluoro Ethers. I. Substitution of  $\alpha$ -Fluorine by Chlorine: The  $\alpha, \alpha, \alpha'$ -Trichloro Perfluoro Ethers. *J. Am. Chem. Soc.*, Vol. 77, Sept. 20, 1955, pp. 4837-4840.
41. Van Dyke Tiers, G.: The Chemistry of Perfluoro Ethers. II. Ether Cleavage with Simultaneous Replacement of  $\alpha$ -Fluorine by Chlorine. *J. Am. Chem. Soc.*, Vol. 77, Sept. 20, 1955, pp. 6703-6704.
42. Van Dyke Tiers, G.: The Chemistry of Perfluoro Ethers. III. Synthesis of  $\omega$ -Trichloromethylperfluoroacyl Chlorides. *J. Am. Chem. Soc.*, Vol. 77, Sept. 20, 1955, pp. 6704-6706.
43. Sianesi, D.; and Fontanelli, R.: Perfluoro Polyethers. Their Structure and Reaction with Aluminum Chloride. *Die Makromolekulare Chemie*, 102, Nr. 2311, 1967, pp. 115-124.

44. Carré, D.J.; and Markowitz, J.A.: The Reaction of PFPE Oil with  $\text{FeF}_3$ ,  $\text{AlF}_3$ , and  $\text{AlCl}_3$  at Elevated Temperatures. ASLE Trans., Vol. 28, 1, pp. 40–46.
45. Zehe, M.J.; and Faut, O.D.: Acidic Attack of PFPE Lubricant Molecules by Metal Oxide Surfaces. NASA TM-101962.
46. Kasai, P.H.; Tang, W.T.; and Wheeler, P.O.: Degradation of PFPE's Catalyzed by Aluminum Oxide. Applied Surface Science, 51, 1991, pp. 201–211.
47. Basu, P.; Ballinger, T.H.; and Yates, J.T., Jr.: Fluoroalkyl Ether Chemistry on Alumina: A Transmission IR Study of the Adsorption and Thermal Decomposition of  $(\text{CF}_2\text{H})_2\text{O}$  on  $\text{Al}_2\text{O}_3$ . Langmuir, Vol. 5, No. 2, p. 198.
48. Cvitkovic, E.; Klaus, E.E.; and Lockwood, F.: A Thin Film Test for Measurement of the Oxidation and Evaporation of Ester Type Lubricants. ASLE Trans., Vol. 22, No. 4, Oct. 1979, pp. 395–401.
49. Lockwood, F.E.; and Klaus, E.E.: Ester Oxidation Under Simulated Boundary Lubrication Conditions. ASLE Trans., Vol. 24, No. 2, Apr. 1981.
50. Morales, W.: HPLC: A Brief Introduction, and Its Application in Analyzing the Degradation of a C-ether. NASA TM-83474, 1983.
51. Medema, J.; Van Bokhoven, J.J.G.; and Kuiper, A.E.T.: Adsorption of Bases on  $\gamma\text{-Al}_2\text{O}_3$ . J. Catal., 25, 1972, pp. 238–244.
52. Herrera-Fierro, P.; Pepper, S.V.; and Jones, W.R., Jr.: An XPS Study of the Stability of Fomblin Z25 on the Native Oxide of Aluminum. NASA TM-105594.
53. Ghosh, A.K.; and Kydd, R.A.: Fluorine-Promoted Catalysts. Catal. Rev. Sci. Eng., 27(4), 1985, pp. 539–589.
54. Flockhart, B.D.; Leith, I.R.; and Pink, R.C.: Trans. Faraday Soc., 65, 1969, p. 542.
55. Flockhart, B.D.; Liew, K.Y.; and Pink, R.C.: Electron Transfer at Alumina Surfaces. J. Catal., 32, 1974, pp. 20–24.

56. Knozinger, H.; and Ratnasamy, P.: Catalytic Aluminas: Surface Models and Characterization of Surface Sites. *Catal. Rev. Sci. Eng.*, 17(1), 1978, pp. 31-70.

## APPENDIX I

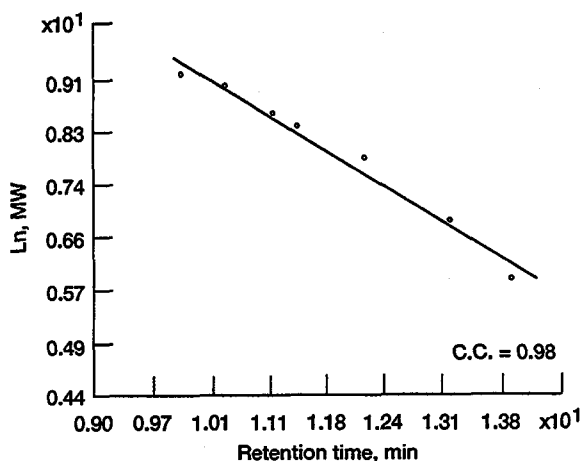
### HIGH PRESSURE LIQUID CHROMATOGRAPHY (HPLC) CALIBRATION

HPLC was used, in this study, in the size exclusion mode. This mode separates a mixture of substances according to their molecular size (geometry) differences by permeation into a solvent-filled matrix in the column. This matrix can be either an inorganic (i.e., silica gel) or organic (i.e., styrene, divinyl benzene) stationary phase. The substances having the greater molecular size will tend not to permeate into the matrix pores as much as the smaller molecular size substances. Thus the order of elution from a size exclusion column is from the larger to the smaller molecular size substances.

A calibration curve can be constructed for a size exclusion column (or set of columns) by plotting the log of the molecular weights of known substances (molecular weight is proportional to molecular size) versus their retention times. By measuring the retention time of an unknown substance, its approximate molecular weight can be estimated.

For this study, the following set of three size exclusion columns was used: two  $\mu$ Bondagel E-125 columns connected in series with a  $\mu$ Porasil 60 Å column. The mobile phase solvent used was 1,1,2-trifluoroethane (TCF) flowing at 0.6 ml/min. A temperature controlled refractive index detector (ERMA ERC-7510) was used to detect the eluted substances. The detector was set at 303 K (30 °C), and the refractive index scale was set to 4X.

A series of perfluorinated substances was used to construct the calibration curve used in this study.



	Retention time, min	MW	Natural log MW
1.	Fomblin Z25	10 200	9.23
2.	Demnum S200	8500	9.05
3.	Demnum S100	5600	8.63
4.	Demnum S65	4550	8.42
5.	Demnum S20	2700	7.90
6.	HFPO Hexamer	963	6.87
7.	Perfluorodiglym	372	5.92

## APPENDIX II

### DIFFERENTIAL SCANNING CALORIMETRY (DSC) CALIBRATION

A DSC thermal unit measures the differential heat flow between a sample and a reference, and these measured values can be plotted as a function of the sample temperature. A Dupont DSC unit was used for this study.

Before using the DSC unit to study the decomposition of PFPE F, the unit had to be calibrated. The calibration entails the calculation of a DSC cell constant. This was done by hermetically sealing 10.68 mg of indium metal between two aluminum sample pans. The sealed pans were then placed on top of a sample constantan (thermocouple) disk located inside the DSC cell. A matching set of sealed aluminum pans (without indium metal) was placed on top of a reference constantan disk. The DSC cell was then covered and flushed with a constant flow of nitrogen gas at 40 ml/min. The DSC unit was then temperature programmed to ramp 10 K/min from room temperature to 473 K (200 °C). The resulting DSC thermogram showed an endothermic peak starting at an onset temperature of 158.3 °C (fig. A1). The melting point of indium is 156.6 °C. This temperature difference was then used by a computer program to calculate a DSC cell constant of 1.3362. A DSC run using indium was then repeated using the calculated cell constant and the mass of the indium metal (10.68 mg). An onset melting temperature of 156.6 °C was recorded (fig. A2), as well as an enthalpy of fusion of 28.28 J/g—the listed value for the enthalpy of fusion for indium is 28.4 J/g.

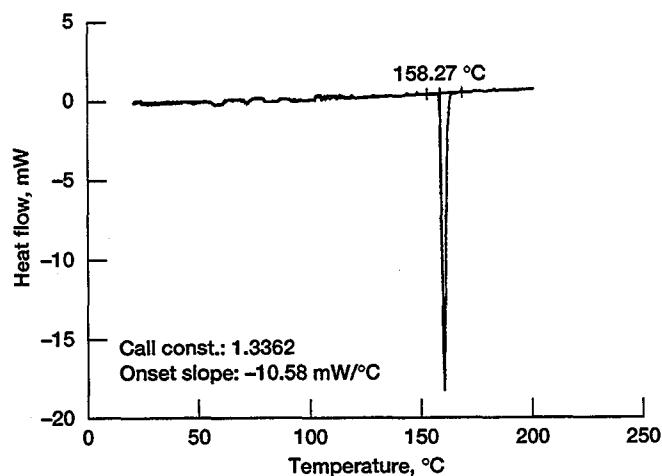


Figure A1

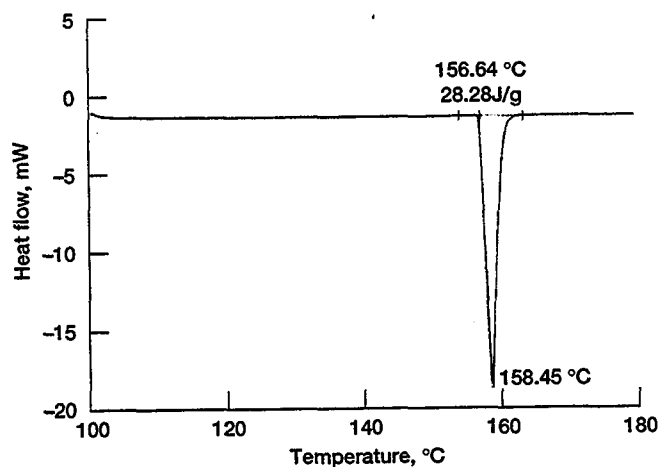


Figure A2

**REPORT DOCUMENTATION PAGE**Form Approved  
OMB No. 0704-0188

Public reporting burden for this collection of information is estimated to average 1 hour per response, including the time for reviewing instructions, searching existing data sources, gathering and maintaining the data needed, and completing and reviewing the collection of information. Send comments regarding this burden estimate or any other aspect of this collection of information, including suggestions for reducing this burden, to Washington Headquarters Services, Directorate for Information Operations and Reports, 1215 Jefferson Davis Highway, Suite 1204, Arlington, VA 22202-4302, and to the Office of Management and Budget, Paperwork Reduction Project (0704-0188), Washington, DC 20503.

1. AGENCY USE ONLY (Leave blank)		2. REPORT DATE April 1994	3. REPORT TYPE AND DATES COVERED Technical Memorandum	
4. TITLE AND SUBTITLE Perfluoropolyalkylether Decomposition on Catalytic Aluminas			5. FUNDING NUMBERS  WU-505-63-5A	
6. AUTHOR(S)  Wilfredo Morales				
7. PERFORMING ORGANIZATION NAME(S) AND ADDRESS(ES)  National Aeronautics and Space Administration Lewis Research Center Cleveland, Ohio 44135-3191			8. PERFORMING ORGANIZATION REPORT NUMBER  E-8697	
9. SPONSORING/MONITORING AGENCY NAME(S) AND ADDRESS(ES)  National Aeronautics and Space Administration Washington, D.C. 20546-0001			10. SPONSORING/MONITORING AGENCY REPORT NUMBER  NASA TM-106547	
11. SUPPLEMENTARY NOTES Responsible person, Wilfredo Morales, organization code 5140, (216) 433-6052.				
12a. DISTRIBUTION/AVAILABILITY STATEMENT  Unclassified - Unlimited Subject Category 23			12b. DISTRIBUTION CODE	
13. ABSTRACT (Maximum 200 words)  The decomposition of Fomblin Z25, a commercial perfluoropolyalkylether liquid lubricant, was studied using the Penn State Micro-oxidation Test, and a thermal gravimetric/differential scanning calorimetry unit. The micro-oxidation test was conducted using 440C stainless steel and pure iron metal catalyst specimens, whereas the thermal gravimetric/differential scanning calorimetry tests were conducted using catalytic alumina pellets. Analysis of the thermal data, high pressure liquid chromatography data, and x-ray photoelectron spectroscopy data support evidence that there are two different decomposition mechanisms for Fomblin Z25, and that reductive sites on the catalytic surfaces are responsible for the decomposition of Fomblin Z25.				
14. SUBJECT TERMS  Perfluoropolyalkylethers; Lewis acids; Space lubrication; Aluminas			15. NUMBER OF PAGES  60	
17. SECURITY CLASSIFICATION OF REPORT Unclassified			18. SECURITY CLASSIFICATION OF THIS PAGE Unclassified	19. SECURITY CLASSIFICATION OF ABSTRACT Unclassified
				20. LIMITATION OF ABSTRACT A04